Atmos. Chem. Phys. Discuss., 12, 30755–30804, 2012
www.atmos-chem-phys-discuss.net/12/30755/2012/
doi:10.5194/acpd-12-30755-2012

Atmospheric Chemistry and Physics Discussions

Preindustrial to present day changes in tropospheric hydroxyl radical and methane lifetime from the Atmospheric Chemistry and Climate Model Intercomparison Project (ACCMIP)

V. Naik[1], A. Voulgarakis[2], A. M. Fiore[3], L. W. Horowitz[4], J.-F. Lamarque[5], M. Lin[4,6], M. J. Prather[7], P. J. Young[8,9,*], D. Bergmann[10], P. J. Cameron-Smith[10], I. Cionni[11], W. J. Collins[12,], S. B. Dalsøren[13], R. Doherty[14], V. Eyring[15], G. Faluvegi[16], G. A. Folberth[12], B. Josse[17], Y. H. Lee[16], I. A. MacKenzie[14], T. Nagashima[18], T. P. C. van Noije[19], D. A. Plummer[20], M. Righi[15], S. T. Rumbold[12], R. Skeie[13], D. T. Shindell[16], D. S. Stevenson[14], S. Strode[21], K. Sudo[22], S. Szopa[23], and G. Zeng[24]**

[1]UCAR/NOAA Geophysical Fluid Dynamics Laboratory, Princeton, New Jersey, USA
[2]Department of Physics, Imperial College, London, UK
[3]Department of Earth and Environmental Sciences and Lamont-Doherty Earth Observatory of Columbia University, Palisades, New York, USA

[4]NOAA Geophysical Fluid Dynamics Laboratory, Princeton, New Jersey, USA
[5]National Center for Atmospheric Research, Boulder, Colorado, USA
[6]Atmospheric and Oceanic Sciences, Princeton University, New Jersey, USA
[7]Department of Earth System Science, University of California, Irvine, California, USA
[8]Cooperative Institute for Research in the Environmental Sciences, University of Colorado-Boulder, Boulder, Colorado, USA
[9]Chemical Sciences Division, NOAA Earth System Research Laboratory, Boulder, Colorado, USA
[10]Lawrence Livermore National Laboratory, Livermore, California, USA
[11]ENEA, Bologna, Italy
[12]Hadley Centre for Climate Prediction, Met Office, Exeter, UK
[13]CICERO, Center for International Climate and Environmental Research-Oslo, Oslo, Norway
[14]School of Geosciences, University of Edinburgh, Edinburgh, UK
[15]Deutsches Zentrum für Luft- und Raumfahrt, Institut für Physik der Atmosphäre, Oberpfaffenhofen, Germany
[16]NASA Goddard Institute for Space Studies, New York City, New York, USA
[17]Météo-France, CNRM/GMGEC/CARMA, Toulouse, France
[18]National Institute for Environmental Studies, Tsukuba-shi, Ibaraki, Japan
[19]Royal Netherlands Meteorological Institute, De Bilt, The Netherlands
[20]Canadian Centre for Climate Modeling and Analysis, Environment Canada, Victoria, British Columbia, Canada
[21]NASA Goddard Space Flight Center, Greenbelt, Maryland, USA and Universities Space Research Association, Columbia, MD, USA
[22]Department of Earth and Environmental Science, Graduate School of Environmental Studies, Nagoya University, Nagoya, Japan
[23]Laboratoire des Sciences du Climat et de l'Environment, Gif-sur-Yvette, France
[24]National Institute of Water and Atmospheric Research, Lauder, New Zealand
[*]now at: Lancaster Environment Centre, Lancaster University, Lancaster, UK
[**]now at: Department of Meteorology, University of Reading, UK

ACPD
12, 30755–30804, 2012

Received: 31 October 2012 – Accepted: 9 November 2012 – Published: 28 November 2012

Correspondence to: V. Naik (vaishali.naik@noaa.gov) and A. Voulgarakis (a.voulgarakis@imperial.ac.uk)

Published by Copernicus Publications on behalf of the European Geosciences Union.

ACPD
12, 30755–30804, 2012

Abstract

We have analysed results from 17 global models, participating in the Atmospheric Chemistry and Climate Model Intercomparison Project (ACCMIP), to explore trends in hydroxyl radical concentration (OH) and methane (CH_4) lifetime since preindustrial times (1850) and gain a better understanding of their key drivers. For the present day (2000), the models tend to simulate higher OH abundances in the Northern Hemisphere versus Southern Hemisphere. Evaluation of simulated carbon monoxide concentrations, the primary sink for OH, against observations suggests low biases in the Northern Hemisphere that may contribute to the high north-south OH asymmetry in the models. A comparison of modelled and observed methyl chloroform lifetime suggests that the present day global multi-model mean OH concentration is slightly overestimated. Despite large regional changes, the modelled global mean OH concentration is roughly constant over the past 150 yr, due to concurrent increases in OH sources (humidity, tropospheric ozone, and NO_x emissions), together with decreases in stratospheric ozone and increase in tropospheric temperature, compensated by increases in OH sinks (methane abundance, carbon monoxide and non-methane volatile organic carbon (NMVOC) emissions). The large intermodel diversity in the sign and magnitude of OH and methane lifetime changes over this period reflects differences in the relative importance of chemical and physical drivers of OH within each model. For the 1980 to 2000 period, we find that climate warming and a slight increase in mean OH leads to a 4.3 ± 1.9 % decrease in the methane lifetime. Analysing sensitivity simulations performed by 10 models, we find that preindustrial to present day climate change decreased the methane lifetime by about 4 months, representing a negative feedback on the climate system. Further, using a subset of the models, we find that global mean OH increased by 46.4 ± 12.2 % in response to preindustrial to present day anthropogenic NO_x emission increases, and decreased by 17.3 ± 2.3 %, 7.6 ± 1.5 %, and 3.1 ± 3.0 % due to methane burden, and anthropogenic CO, and NMVOC emissions increases, respectively.

ACPD

12, 30755–30804, 2012

1 Introduction

The hydroxyl radical (OH) is the dominant oxidizing agent in the global troposphere as it reacts with most pollutants (Levy, 1971; Logan et al., 1981; Thompson, 1992), thereby controlling their atmospheric abundance and lifetime. Any changes in OH affect the tropospheric chemical lifetime of methane (CH_4), the most abundant organic species in the atmosphere and a potent greenhouse gas. Complex series of chemical reactions involving tropospheric ozone (O_3), methane, carbon monoxide (CO), non-methane volatile organic compounds (NMVOCs), and nitrogen oxides ($NO_x = NO + NO_2$), as well as the levels of solar radiation and humidity, determine the tropospheric abundance of OH (Logan et al., 1981; Thompson, 1992). Reaction with OH determines the chemical lifetime of methane as it is the primary mechanism by which methane is removed from the atmosphere. The more-than-doubling of global methane abundance since preindustrial times (Petit et al., 1999; Loulergue et al., 2008; Sapart et al., 2012), combined with the rise in emissions of NO_x, CO and NMVOCs (Lamarque et al., 2010), is likely to have had some influence on OH and consequently on the chemical methane lifetime in the past 150 yr. We analyse results from global chemistry-climate models participating in the Atmospheric Chemistry and Climate Model Intercomparison Project (ACCMIP; see www.giss.nasa.gov/projects/accmip) to investigate the changes in tropospheric OH abundance and its drivers, and methane lifetime over the historical period between 1850 and 2000.

Primary production of tropospheric OH occurs when electronically excited $O(^1D)$ radicals, produced by ozone photolysis at wavelengths less than 340 nm, react with water. Therefore, OH concentrations are highest in the tropical lower to middle troposphere, reflecting the combined impact of high levels of water vapour, and low stratospheric ozone column, meaning higher incident ultraviolet (UV) radiation (Logan et al., 1981; Spivakovsky et al., 2000; Lelieveld et al., 2002). OH has a tropospheric lifetime of a second, reacting rapidly with CO, methane and NMVOCs to produce HO_2 or an organic peroxy radical (RO_2), key species for the secondary production of OH. Secondary

ACPD
12, 30755–30804, 2012

formation of OH can occur in the presence of NO_x since NO reacts with HO_2 or RO_2 to recycle OH (Crutzen, 1973; Zimmerman et al., 1978). Additional OH is produced because NO_2 can photolyse resulting in the formation of ozone, the primary precursor to OH (Hameed et al., 1979). This secondary production of OH via radical recycling by NO_x plays a more important role at higher latitudes where incoming solar radiation and water vapour are less abundant, and NO_x and ozone concentrations are generally higher (Logan et al., 1981; Spivakovsky et al., 2000; Lelieveld et al., 2002). Conversely, in clean air the reaction chain can be terminated by the formation of H_2O_2 resulting in the loss of OH. Recent work suggests that OH can also be produced in unpolluted forested low-NO_x environments where the reactions of the oxidation products of biogenic NMVOCs directly recycle OH radicals (Lelieveld et al., 2008; Peeters et al., 2009), though the extent to which OH can be recycled is still in question (Mao et al., 2012a). Chemical mechanisms describing this phenomenon are not implemented in the models considered here. Temperature plays a key role by controlling reaction rates and tropospheric water vapour abundances. Overall, the global mean tropospheric OH represents a balance between its sources (water vapor, tropospheric ozone, NO_x) and sinks (methane, CO, NMVOCs), that is modulated by overhead ozone column (UV radiation) and temperature.

The extent to which tropospheric OH level has changed due to anthropogenic activity is highly uncertain. Observational evidence of preindustrial to present day changes in OH is sparse and questionable. For example, Staffelbach et al. (1991) postulated that OH has decreased by 30 % in the present day relative to preindustrial times using measurements of formaldehyde to methane ($HCHO/CH_4$) ratio in ice cores as potential proxy of the past OH concentration. However, Sofen et al. (2011) note that ice-core formaldehyde is sensitive to post-depositional processing that impedes quantitative interpretation of past atmospheric conditions. Previous modelling of changes in tropospheric mean OH abundance from preindustrial to present day range from increases of 6–15 % (Crutzen and Bruhl, 1993; Martinerie et al., 1995; Berntsen et al., 1997), to no change (Pinto and Khalil, 1991; Lelieveld et al., 2004), to decreases of 5–33 %

ACPD
12, 30755–30804, 2012

(Thompson et al., 1992; Wang and Jacob, 1998; Mickley et al., 1999; Hauglustaine and Brasseur, 2001; Grenfell et al., 2001; Lelieveld et al., 2002; Shindell et al., 2003, 2006a; Wong et al., 2004; Lamarque et al., 2005a; Skeie et al., 2010; Sofen et al., 2011; John et al., 2012). As evident from these wide-ranging results, there is no consensus on how tropospheric OH abundance has evolved in the past 150 years, with a consequent lack of agreement on the trends in methane lifetime during the historical period (Table 1 of John et al., 2012).

Much effort has been placed on understanding the long-term trends and interannual variability in atmospheric OH concentrations over the past two to three decades using measurements of trace gases whose emissions are well known and whose primary sink is OH. Accurate long-term measurements of the industrial chemical 1,1,1-trichloroethane (methyl chloroform CH_3CCl_3) (Prinn et al., 1995, 2000, 2001; Montzka et al., 2000) in the atmosphere and an assumption of accurate emissions inventories (Montzka and Fraser, 2003) enable estimates of trends and interannual variability in tropospheric abundance of OH to be inferred from observed changes in CH_3CCl_3 (Prinn et al., 1995, 2001; Krol et al., 1998; Krol and Lelieveld, 2003; Bousquet et al., 2005; Montzka et al., 2000, 2011). Large changes in OH in the past three decades inferred from CH_3CCl_3 observations (Prinn et al., 2001; Bousquet et al., 2005) have been debated in the literature (Krol and Lelieveld, 2003; Lelieveld et al., 2004) as they have been difficult to reconcile based on results from current theoretical models that suggest small increases in global OH concentrations for the 1980–2000 period (Karlsdttir and Isaksen, 2000; Dentener et al., 2003; Dalsøren and Isaksen, 2006; John et al., 2012; Holmes et al., 2012). In a more recent analysis of CH_3CCl_3 measurements since 1998 (a period with diminished atmospheric CH_3CCl_3 gradient from Montreal Protocol induced phasing out of its emissions), Montzka et al. (2011) infer small interannual OH variability and attribute previously estimated large year-to-year OH variations before 1998 to uncertainties in CH_3CCl_3 emissions. Further, using observations of methane and $\delta^{13}C-CH_4$, Monteil et al. (2011) find that moderate ($< 5\%$) increases in global OH are needed to explain the observed slowdown in the growth rate of atmospheric

ACPD
12, 30755–30804, 2012

methane, thus incompatible with the previously estimated observation-based reduction in OH in 2000 relative to 1980.

Previous multi-model studies have focused on inter-comparison of changes in atmospheric composition with reference to OH and methane lifetime in the context of changes in ozone and CO (Stevenson et al., 2006; Shindell et al., 2006b). Here our goals are to (1) evaluate the present day (2000) OH simulated by global models participating in ACCMIP, (2) apply results over the 1850–2000 period to explore trends in OH and methane lifetime since preindustrial times, (3) better understand the key drivers of the simulated trends over this time period, and finally (4) investigate the impact of individual driving factors (climate and ozone precursor emissions) on OH and methane lifetime. A parallel study compares future projections of OH and methane lifetime in the ACCMIP models (Voulgarakis et al., 2012). We provide a summary of models used, the experiments they performed and our analysis approach in Sect. 2. Historical evolution of OH and methane lifetime is presented in Sect. 3. Changes in OH, methane lifetime, and their driving factors in the present day (2000) relative to preindustrial (1850) and to 1980 are discussed in Sects. 4 and 5, respectively. The sensitivity of OH and methane lifetime to historical change in climate, and changes in methane burden and emissions are presented in Sects. 6 and 7, respectively. Finally, conclusions are drawn in Sect. 8.

2 Methodology

2.1 ACCMIP Models

We analyse results from 17 different global models to investigate the historical evolution (1850–2000) of OH and methane lifetime. ACCMIP results have also been analysed to compare the historical to future evolution of atmospheric composition with focus on the tropospheric ozone (Young et al., 2012), and its radiative forcing (Stevenson et al., 2012; Bowman et al., 2012), black carbon (Lee et al., 2012), and aerosol radiative

ACPD
12, 30755–30804, 2012

forcing (Shindell et al., 2012). Detailed descriptions of ACCMIP models are provided by Lamarque et al. (2012).

Nearly all the models are run as coupled chemistry-climate models (CCMs), driven by climatological monthly mean sea-surface temperatures (SSTs) and sea-ice coverage (SIC) either from observations or from the corresponding coupled ocean-atmosphere model integrations submitted to the Coupled Model Intercomparison Project Phase 5 (CMIP5). Three models, namely CICERO-OsloCTM2, MOCAGE, and TM5 are chemistry-transport models (CTMs) driven by meteorological fields from an offline reanalysis or output from a general circulation model. Meteorological fields used to run CICERO-OsloCTM2 and TM5 did not vary across time-slice simulations. GISS-E2-R and GISS-E2-R-TOMAS are two different configurations of the same model – GISS-E2-R is a fully interactive coupled ocean-atmosphere-chemistry model with a simple mass-based representation of aerosols while GISS-E2-R-TOMAS uses SSTs and SIC from GISS-E2-R with a more detailed aerosol microphysics scheme. Similarly, HadGEM2 and HadGEM2-ExtTC are the same, except HadGEM2 includes a simple tropospheric chemistry scheme, while HadGEM2-ExtTC incorporates a more detailed chemistry scheme with many more hydrocarbons.

Key characteristics of the models relevant for simulating atmospheric OH and methane lifetime are presented by Voulgarakis et al. (2012). Briefly, anthropogenic and biomass burning emissions are taken from Lamarque et al. (2010) and vary over the historical period (Young et al., 2012). Natural emissions for NO_x, CO, and NMVOCs were specified from different sources and are one of the major sources of diversity in model results (source-wise emissions for 2000 are summarized in Table S1). Other sources of differences across the models are expected to result from diversity in the complexity of NMVOC chemistry (mechanisms include a range from 16 to 100 species), stratospheric ozone representations and resulting impacts on ozone photolysis rates (see Table A1 of Voulgarakis et al. (2012) for further details). Most models prescribe methane values at the surface (but allow it to undergo chemical processing elsewhere in the atmosphere) from the historical reconstruction of Meinshausen et al. (2011)

ACPD
12, 30755–30804, 2012

though a few models use alternative approaches. Two models (STOC-HadAM3 and UM-CAM) apply a uniform global concentration and another (LMDzORINCA) applies emission fluxes. The rate coefficient (k_{CH_4+OH}) for methane oxidation applied in most models is from Sander et al. (2011). The impact of differences in temperature across models on k_{CH_4+OH} is minimal and is, therefore, unlikely to contribute to the diversity in methane lifetime shown later.

2.2 Simulations

We analysed three time-slice simulations over the historical period – 1850, 1980 and 2000, performed by 16 models (HadGEM2-ExtTC performed only attribution simulations described below). The models were typically run for 4 to 10 yr for each time-slice, though GEOSCCM performed 14 yr integrations, CICERO-OsloCTM2 and TM5 performed single year simulations (the reference year for TM5 present day simulation being 2006), and GISS-E2-R and LMDzORINCA were run transiently for the entire historical period. For the analysis performed here, we averaged results over all the available years of each of the three historical time-slices. In the case of the GISS-E2-R and LMDzORINCA models, we averaged years centered on the time-slice (except average over 1850–1859 was used for 1850 and average over 1996–2000 was used for 2000 for LMDzORINCA). Interannual variability in OH is not explicitly addressed here because ACCMIP simulations were designed to address only long-term changes.

Of the 17 models, 10 models performed an additional simulation (Em2000Cl1850) with emissions fixed at 2000 levels, but with climate (SSTs and SIC) set to 1850 conditions (well-mixed greenhouse gases, including methane and ozone depleting substances (ODSs) were also set to 1850 levels for radiation calculations). The difference of Em2000Cl1850 from the 2000 simulation allows us to investigate the influence of historical climate change on global OH and the methane lifetime. Furthermore, a few of these models performed a series of attribution experiments, specifically designed to ascribe ozone and OH changes to the increases in anthropogenic emissions of individual

ACPD
12, 30755–30804, 2012

species (NO_x, CO, NMVOCs) and to the rise in methane concentrations (Stevenson et al., 2012).

2.3 Analysis approach

We calculate the tropospheric methane lifetime against loss by OH (τ_{CH_4}) as the ratio of the global atmospheric methane burden (B_{CH_4}) and the global annual mean tropospheric methane oxidation flux (L_{CH_4}) provided by each model for each year and then averaged over the number of years for each time-slice. Hereafter, "methane lifetime" refers to the lifetime against loss by tropospheric OH. The total methane lifetime additionally includes the small stratospheric and soil sinks (Prather et al., 2001; Stevenson et al., 2006). For tropospheric global budgets, we define the troposphere to extend from the surface to a fixed pressure level of 200 hPa on each model's native vertical grid. We calculated methane lifetime with the tropopause defined as air with ozone concentrations less than or equal to 150 ppbv in the 1850 time-slice simulation (Stevenson et al., 2006; Young et al., 2012) and found it to be within 3 % of the values obtained with the tropopause at 200 hPa. Thus, we conclude that the definition of the tropopause has minimal effect on the calculated methane lifetime. With the exception of global budget terms, we weight global mean quantities reported here by the mass of air in the troposphere for each model.

We also calculate the tropospheric lifetime of CH_3CCl_3 against OH loss as a means of testing model simulated global mean tropospheric OH concentrations for present day. Since models did not simulate the chemistry and distribution of CH_3CCl_3, we calculate its tropospheric lifetime by scaling the methane lifetime with the ratio of the rate coefficient of the reactions of methane and CH_3CCl_3 with OH (Prather and Spivakovsky, 1990) integrated from the surface to the tropopause, as, $\tau_{CH_3CCl_3} = \tau_{CH_4} \frac{\int_{sfc}^{trop} k_{CH_4+OH}(T)}{\int_{sfc}^{trop} k_{CH_3CCl_3+OH}(T)}$, where, $k(T)$, the temperature-dependent rate coefficient for the oxidation of CH_3CCl_3 by tropospheric OH, is $1.64 \times 10^{-12} \exp(-1520/T)\,\mathrm{molec}^{-1}\,\mathrm{cm}^3\,\mathrm{s}^{-1}$ (Sander et al., 2011). We apply monthly mean 3-dimensional temperature as diagnosed by each model to

ACPD
12, 30755–30804, 2012

calculate this rate coefficient. The derived tropospheric chemical lifetime of CH_3CCl_3 is referred to as "CH_3CCl_3 lifetime" here and does not include the small stratospheric and oceanic losses (Prinn et al., 2005; Prather et al., 2012).

3 Historical evolution of OH and methane lifetime

Table 1 shows the historical evolution of the annual mean global total methane burden, tropospheric OH and methane lifetime for the 16 global models. The global methane burden increases by more than a factor of two from 1850 to 2000 in all models. Simulated methane abundances are not sensitive to how methane was prescribed in the models (Lamarque et al., 2012). Despite similar imposed changes in emissions, specifically increases in the emissions of NO_x (OH source), CO and NMVOCs (OH sinks) (Young et al., 2012), and in the methane burden over the 1850 to 2000 period, the models simulate different trends in OH. Models can be categorized into two groups, one with increasing trends in OH (decreasing methane lifetime; bold entries in Table 1; six models) and another with decreasing OH (increasing methane lifetime; plain text in Table 1; nine models). All models simulate larger increases or smaller decreases in tropospheric OH abundance in the Northern Hemisphere (NH) compared to the Southern Hemisphere (SH) consistently from 1850 to 2000 (Table 2). We explore the changes in OH, methane lifetime and their driving factors for present day relative to preindustrial and to 1980 in Sects. 4 and 5, respectively in an attempt to identify the key processes responsible for the different OH trends.

3.1 Evaluation of present day OH

Accurate global-scale measurements of tropospheric OH are a challenge because of its enormous temporal and spatial variability; hence lifetimes of methane and CH_3CCl_3 against reaction with tropospheric OH provide the best constraints on the global mean tropospheric OH concentration. We compare present day (2000) methane and

ACPD
12, 30755–30804, 2012

CH_3CCl_3 lifetimes obtained from models against observationally-derived estimates to evaluate the global mean OH concentrations simulated by the models. The multi-model mean methane lifetime against OH loss of 9.7 ± 1.5[1] yr (Table 1) is about 5 % lower than the mean 1978–2004 tropospheric methane lifetime of $10.2^{+0.9}_{-0.7}$ yr estimated by Prinn et al. (2005), and is about 13 % lower than the most up-to-date observationally-derived estimate of 11.2 ± 1.3 yr for 2010 (Prather et al., 2012). It is identical to the methane lifetime of 9.7 ± 1.7 years obtained from previous multi-model analysis (Shindell et al., 2006b), and is about 5 % lower than the 10.2 ± 1.7 yr reported in the recent Hemispheric Transport of Air Pollution (HTAP) multi-model study (Fiore et al., 2009). The variation in methane lifetime across participating models is about the same as that across the previous multi-model estimates (Shindell et al., 2006b; Fiore et al., 2009). Similarly, the multi-model mean CH_3CCl_3 lifetime of 5.7 ± 0.9 yr (Table 1), is about 5 % lower than the observationally-derived tropospheric lifetime of $6.0^{+0.5}_{-0.4}$ yr over the period 1978–2004 (Prinn et al., 2005), and is about 10 % lower than the recent estimate of 6.3 ± 0.4 yr (Prather et al., 2012) obtained using CH_3CCl_3 observations over the period 1998–2007 (Montzka et al., 2011). This comparison suggests that the multi-model mean present day global tropospheric OH abundance of $11.1 \pm 1.6 \times 10^5$ molec cm^{-3} is overestimated by 10 % but is within the uncertainty range of observations.

Large intermodel spread in the simulated present day global mean tropospheric OH concentrations (and methane and CH_3CCl_3 lifetimes) may be attributed to the diversity in natural emissions, and the unique chemical and dynamical characteristics of the individual models. For example, lowest tropospheric mean OH in UM-CAM most likely stems from its offline photolysis scheme that does not account for changes in clouds, overhead ozone column, or aerosols, resulting in very low photolysis rates and OH (Voulgarakis et al., 2012). The highest tropospheric mean OH abundances are simulated by the CESM-CAM-superfast and MOCAGE models. The representation of NMVOCs is minimal in CESM-CAM-superfast model as it includes isoprene only, thus

[1] Slightly different from that reported by Voulgarakis et al. (2012) as we have included results from GISS-E2-R-TOMAS and TM5.

ACPD
12, 30755–30804, 2012

simulating a smaller sink for OH. Even though MOCAGE has the highest NMVOC emissions, thus a bigger OH sink (Table S1), other factors contribute to its high OH, including the lack of inclusion of aerosol photochemical effects in the model (Bousserez et al., 2007). In addition, low stratospheric ozone columns in MOCAGE may enhance UV radiation resulting in greater OH production in the southern Tropics, although it is difficult to diagnose this as photolysis rates are not available from MOCAGE. Availability of key OH diagnostics from all models participating in future multi-model intercomparison projects will facilitate a better understanding of differences in OH distributions across models.

The present day multi-model mean OH inter-hemispheric (N/S) ratio is 1.28 ± 0.1, in contrast to the range of N/S values derived from measurements of CH_3CCl_3 encompassing the 1980 to 2000 period (Montzka et al., 2000; Prinn et al., 2001; Krol and Lelieveld, 2003; Bousquet et al., 2005). For example, with CH_3CCl_3 measurements for 1998–1999, Montzka et al. (2000) estimate that annual mean OH concentrations are 15 ± 10 % higher south of the inter-tropical convergence zone (ITCZ) than north of it, while Prinn et al. (2001) derive annual mean OH concentrations that are 14 ± 35 % higher in the SH than the NH over the 1978–2000 time period. These observational estimates of N/S OH ratio are highly uncertain as they rely on the assumption of accurate CH_3CCl_3 emission estimates and its atmospheric observations. Nevertheless, these estimates are consistent with present day ozone distributions in the ACCMIP models that are biased high and low in NH and SH, respectively, against satellite and ozonesonde observations (Young et al., 2012). The models thus overestimate OH production from ozone in the NH relative to SH. We test if OH sinks may also be too low in the NH compared with the SH, by evaluating the distribution of CO simulated in the ACCMIP models against observations in the following section.

3.2 Comparison of present day CO with observations

CO is the major sink of tropospheric OH (Jacob, 1999), hence, any biases in CO will likely influence the distribution of OH. Here, we compare annual mean CO from the

ACPD
12, 30755–30804, 2012

models with surface CO measurements averaged over the 1996–2005 period from the NOAA Global monitoring Division (GMD) Carbon Cycle Cooperative Global Air Sampling Network (Novelli and Masarie, 2010) for 50 sites (Fig. 1a) and with the observed mean 2000–2006 CO distribution at 500 hPa from the Measurements of Pollution In The Troposphere (MOPITT) instrument (Fig. 1b). For comparison with surface observations, we sampled model results at pressure levels closest to the pressure altitude, latitude and longitude of the observation sites. For comparison with MOPITT CO, we used monthly mean daytime values derived from version 4 (V4) level 3 retrievals from March 2000 to December 2006 provided at a horizontal resolution of $1^\circ \times 1^\circ$ and at 10 retrieval levels (Deeter et al., 2010). For proper comparison, we transformed each model's CO by first interpolating it to the MOPITT grid and then applying the averaging kernel and a priori profile associated with each MOPITT retrieval (Shindell et al., 2006b; Emmons et al., 2009). A priori profiles associated with V4 are based on a monthly climatology from the global chemical transport model MOZART-4. Detailed evaluation of MOPITT V4 CO retrievals between 2002 and 2007 with in situ measurements show biases of less than 1 % at the surface, 700 hPa and 100 hPa and a bias of about −6 % at 400 hPa (Deeter et al., 2010).

The multi-model mean underestimates the observed surface CO concentrations at most sites in the NH (Fig. 1a), with strong negative biases (up to 60 ppbv) at many high latitude sites. Negative biases persist at the northern mid-latitude sites albeit with smaller magnitudes than those for the northern high-latitude sites. In the SH, the multi-model mean is within ±2 ppbv at most sites. Consistent with the surface CO comparison, the multi-model mean underestimates the MOPITT CO at 500 hPa throughout the NH, except over North India and South-Central China (Fig. 1b). The overestimate over these South Asian regions is present in all models (Fig. S1) and is particularly dominant in the comparison for September (not shown), indicating excessive transport and/or emissions. The multi-model mean CO reproduces the MOPITT values over much of the SH, except over Central Africa, Western South America, Indonesia and surrounding Indian and Pacific oceans possibly related to discrepancies in biomass

ACPD
12, 30755–30804, 2012

burning emissions (Fig. 1b). Despite these regional biases, the models capture the overall spatial distribution of MOPITT CO fairly well as indicated by the high values of spatial correlation coefficients (Table 3).

The multi-model mean CO concentrations generally agree better with observations in the SH, and are biased low in the NH, similar to the earlier multi-model results of Shindell et al. (2006b). The simulated low CO levels in the NH are consistent with a weaker-than-observed OH sink that contributes to the larger OH north-to-south asymmetry compared to that derived from CH_3CCl_3 observations.

4 Preindustrial to present day changes in OH and methane lifetime, and their driving factors

We now explore the changes in OH from preindustrial to present day and their driving factors. The multi-model tropospheric mean OH oxidative capacity has remained nearly constant over the past 150 yr (Table 4). Globally, the increases in the sources of OH – humidity (4.7±2.6 %), tropospheric ozone (38±10.8 %; Young et al., 2012) and NO_x (as $NO + NO_2$) burden (108.0 ± 75.4 %), decreases in stratospheric ozone (−4.5 ± 4.8 %), which modulate tropospheric ozone photolysis rates, and increase in tropospheric temperature (0.8±0.4 K), are compensated by increases in OH sinks – doubling of methane (Table 1) and CO burdens (Table 4). The near constant global mean OH over the historical period is consistent with the findings of Lelieveld et al. (2002; 2004). Large intermodel spread in the simulated changes in OH exists, ranging from a decrease of 12.7 % (GEOSCCM) to an increase of 14.6 % (MOCAGE) (Table 4). It is notable that with the consistent ACCMIP modeling specifications, the preindustrial to present day percent changes in OH for all ACCMIP models are within ±15 %, a range significantly reduced from the previously published model estimates of preindustrial to present day OH changes (Table 1 of John et al., 2012).

We now discuss regional changes in annual mean OH by relating them to regional changes in chemistry (CO, NO_x burdens, stratospheric ozone) and climate drivers

ACPD
12, 30755–30804, 2012

(humidity and temperature) of OH. Preindustrial to present day changes in multi-model mean OH, CO and NO_x burdens, humidity and temperature for 12 tropospheric subdomains, as defined by Lawrence et al. (2001), are shown in Fig. 2 (left column). Strong intermodel diversity exists in the magnitude of NO_x burden changes, particularly in the upper troposphere (Fig. 2e), possibly reflecting the model-to-model differences in processes that dominate the response in this region and the uncertainty associated with natural NO_x emissions. The intermodel diversity in CO, humidity and temperature changes is much lower compared to that for NO_x changes. Strong intermodel variation exists in both the sign and magnitude of regional preindustrial to present day changes in OH (see Fig. S2 for regional OH changes in individual models). For many atmospheric regions, the standard deviation in OH change across models is greater than the multi-model mean change (Fig. 2a) suggesting that the changes are not statistically significant. The NH lower tropospheric (surface to 750 hPa) extra-tropics (30°–90° N) is the only region of the atmosphere where the models agree on the sign of OH change (increase), and its magnitude appears to be statistically significant (multi-model mean greater than standard deviation). This is also the region with the largest increases in CO and NO_x burdens (Figs. 2c, e), driven by the changes in anthropogenic emissions which are the same in all the models. Humidity levels increase everywhere (Fig. 2g) in response to temperature increases (Fig. 2k). Strong increases in tropospheric ozone, the primary source of OH, are also simulated in the NH lower troposphere in response to emission increases (Young et al., 2012). Thus, combined increases in water vapor, ozone and NO_x outweigh CO increases resulting in enhanced OH levels in the NH extra-tropical lower troposphere in the present day relative to preindustrial.

Reflecting the changes in OH, there is a large intermodel variability in the preindustrial to present day change in methane lifetime (Table 4) with increase of 12 % (GEOSCCM) to decrease of 14.1 % (NCAR-CAM3.5). Changes in methane lifetime for each model are inversely proportional to the OH change in the model, except for HadGEM2 which shows no change in OH.

ACPD
12, 30755–30804, 2012

4.1 Diversity in preindustrial to present day changes

We find that intermodel variation in the sign and magnitude of the preindustrial to present day change in global mean OH correlates strongly with the ratio of tropospheric CO and NO_x burden changes (Fig. 3; $r^2 = 0.7$). Models that simulate decreases in present day global mean OH relative to preindustrial have stronger increases in global CO compared with NO_x burdens (except HadGEM2), while models that simulate increase in OH show larger relative increases in NO_x versus CO burdens (except GISS-E2-R and GISS-E2-R-TOMAS) (Table 4). Removing the outlier model, HadGEM2, increases the coefficient of determination (r^2) to 0.8. The correlation is particularly tight for models that simulate preindustrial to present day OH decreases.

The diversity in the CO/NO_x ratios across models reflects not only the uncertainties in emissions, particularly natural emissions of NO_x, CO and NMVOCs, but also how their chemistry and transport is represented in the models. To advance our understanding of the evolution of atmospheric OH, better observational constraints on the distribution of these trace species and the key processes controlling their distributions in different regions of the world are needed. Furthermore, concerted efforts to evaluate tropospheric chemistry schemes implemented in the models (Archibald et al., 2010; Barkley et al., 2011) are also needed to make progress in understanding the diversity in OH distributions and changes across models.

5 1980 to 2000 changes in OH and methane lifetime

Consistent with prior modelling studies (Karlsdttir and Isaksen, 2000; Dentener et al., 2003; Dalsøren and Isaksen, 2006; John et al., 2012; Holmes et al., 2012), the multi-model mean OH increases slightly from 1980 to 2000 by 3.5 ± 2.2 % (Table 5). Over this period, increases in OH sinks, specifically the methane (12 ± 1.9 %) and CO (5.2 ± 2.0 %) burdens are slightly outweighed by increases in humidity (2.8 ± 1.3 %), NO_x burdens (4.3 ± 12.3 %), and stratospheric ozone loss (3.1 ± 2.3 %). In contrast to

ACPD
12, 30755–30804, 2012

the disagreement in the sign of OH change for the 1850–2000 period, all models agree on a small OH increase from 1980 to 2000. The multi-model mean methane lifetime decreases by 4.3 ± 1.9 % from 1980 to 2000 reflecting the small increase in tropospheric OH and warming of 0.4 ± 0.2 K. While the models are consistent with each other, the observational estimates of trends in OH derived from CH_3CCl_3 measurements indicate a ∼ 10 % decrease over a similar period (Prinn et al., 2001; Bousquet et al., 2005). More recent analysis of CH_3CCl_3 observations over the 1998–2007 period indicates that global OH is well-buffered against perturbations (Montzka et al., 2011) and suggests that the uncertainties in CH_3CCl_3 data before 1998 may have led to artificially large OH trends reported in previous studies.

Regionally, the NH shows larger OH increases (4.6 ± 1.9 %) (Fig. 2b) than the SH (2.2 ± 3.2 %), the latter being where intermodel variability is large (Fig. S3). The largest increases occur in the NH extra-tropical troposphere (Fig. 2b), which coincide with increases in humidity (Fig. 2h), and decreases in the CO burden (Fig. 2f). NO_x burdens decrease in the extra-tropical NH lower troposphere in 2000 relative to 1980, possibly driven by decreasing North American and European emissions (Lamarque et al., 2010; Granier et al., 2011). The large intermodel diversity in the sign of change in the SH may be related to the extent of stratospheric ozone loss and its influence on photolysis as simulated by the models. For example, GISS-E2-R with an interactive photolysis scheme and strong stratospheric ozone loss from 1980 to 2000 (not shown) simulates the strongest increase in SH OH, particularly in the extra-tropical troposphere (Fig. S3). The unique chemical and dynamical characteristics of individual models drive the range of OH trends (∼ 0 to 7 %) for the 1980–2000 period obtained here.

6 Sensitivity of OH and methane lifetime to climate

In this section, we investigate the influence of climate change on OH and methane lifetime by analysing the simulations performed by 10 models with 2000 emissions but driven by 1850s climate (Em2000Cl1850). We compare the base 2000 time-slice and

ACPD
12, 30755–30804, 2012

Em2000CI1850 simulations to diagnose the impact of climate change from 1850 to 2000.

Preindustrial to present day climate change causes a multi-model mean global OH increase of 2.1 ± 2.0 % (Fig. 4) and a methane lifetime decrease of 0.30 ± 0.2 yr (Table 6). All models, except GFDL-AM3, simulate OH increases (Fig. 4) and methane lifetime decreases (Table 6) in response to historical climate change. GISS-E2-R produces the strongest methane lifetime decrease, while STOC-HadAM3 produces the strongest methane lifetime decrease per unit temperature increase. Increases in water vapour cause tropospheric OH increases, particularly in the upper troposphere where the relative increases in humidity (Fig. 5a) are greatest. Warmer temperatures and increased OH enhance oxidative loss of methane (Fig. 5c), decreasing the methane lifetime by 0.30 ± 0.24 yr (Table 6) and representing a small negative climate feedback, in agreement with prior studies (Stevenson et al., 2000, 2006; Johnson et al., 2001; Voulgarakis et al., 2012).

7 Attribution of OH changes to methane burden and NO_x, CO, and NMVOC emissions

A subset of the models performed a series of attribution experiments with 2000 climate conditions but with anthropogenic CO, NO_x and NMVOC emissions, and methane concentrations individually set to preindustrial levels. For the methane attribution experiment performed by eight models (Em2000CH41850), the methane concentration was fixed at an 1850s level (791 ppbv), while for the emissions attribution experiments (Em2000CO1850, Em2000NOx1850, and Em2000NMVOC1850) conducted by six models, methane was fixed at 2000s level (1751 ppbv) and anthropogenic emissions were reduced to their 1850 values separately for each simulation. We subtract results of each perturbation simulation from the base 2000 time-slice simulation to diagnose the impact of preindustrial (1850) to present day (2000) changes in each of the specific drivers on OH, as shown in Fig. 4. Because methane concentrations were

ACPD
12, 30755–30804, 2012

prescribed (rather than using emissions), these attribution simulations are not at steady state with respect to methane concentration and, therefore, OH (Prather, 1994, 1996; Fuglestvedt et al., 1999; Derwent et al., 2001; Wild et al., 2001; Stevenson et al., 2004; Naik et al., 2005; Shindell et al., 2005, 2009; West et al., 2007; Fiore et al., 2008). Here, we only diagnose instantaneous changes in methane lifetime; steady-state changes are addressed by Stevenson et al. (2012).

The largest change in global mean OH is simulated for preindustrial to present day increases in anthropogenic NO_x emissions, followed by increases in methane concentrations, while smaller changes result from increases in CO and NMVOCs emissions across the subset of models (Fig. 4). Global mean OH increases by 46.4 ± 12.2 % due to NO_x emission increases as a result of increases in both primary and secondary OH production. The more than a factor of two increases in methane concentrations at present day NO_x levels leads to increases in tropospheric ozone, the primary source of OH. However, OH is consumed during the oxidation of methane and its oxidation products, so that the net result is a global OH decrease of 17.3 ± 2.3 %. Smaller decreases in mean OH occur in response to anthropogenic CO (7.6 ± 1.5 %) and NMVOC emission (3.1 ± 3.0 %) increases (Fig. 6). Despite being the major OH sink, the decrease in OH from CO increase is smaller than that from methane increase because CO has a buffering impact from increasing ozone and hydrogen peroxide (Leibensperger et al., 2011).

Methane lifetime also responds most strongly to increases in NO_x, followed by methane, CO and NMVOC, respectively. However, the response in the perturbation lifetime is different when the non-linear feedback of methane on its own lifetime is considered (Stevenson et al., 2012). Furthermore, the sum of OH/methane lifetime changes diagnosed from the individual attribution experiments performed by a model is not equal to the total preindustrial to present-day diagnosed from the historical time-slice simulations (Table 4). This is partly because of the inherent non-linear chemical system and partly because all the offsetting processes influencing OH in the coupled chemistry-climate system are not included in these attribution experiments.

ACPD
12, 30755–30804, 2012

Regionally, OH reductions are slightly stronger in the SH compared with the NH in response to methane changes (Fig. 6a) since methane is a more important OH sink in the SH than in NH (Spivakovsky et al., 2000). On the other hand, OH decreases are stronger in the NH compared with SH for CO and NMVOC emission increases (Fig. 6b, d), reflecting higher anthropogenic sources in the NH. Increases in anthropogenic NO_x emissions produce the largest inter-hemispheric asymmetry in the OH response (Fig. 6c).

Intermodel diversity in the response of OH to methane and CO perturbations is small, compared with that for NMVOC and NO_x perturbations (Fig. 6). Significant diversity in the sign and magnitude of OH change for different tropospheric regions due to NMVOC emissions (Fig. 6d) reflect the differences in chemistry schemes implemented in the models and uncertainties in natural emissions. The response of OH to NMVOCs, particularly biogenic NMVOCs, is an area of active research (Lelieveld et al., 2008; Paulot et al., 2009; Peeters et al., 2009; Barkley et al., 2011) and efforts that combine observations and modeling activities can help in alleviating uncertainties in our understanding.

8 Conclusions

We have investigated the historical (1850–2000) evolution of global hydroxyl (OH) radical and methane lifetime by analysing results from 17 global chemistry-climate models. We determined a multi-model mean present day (2000) tropospheric methane lifetime of 9.7 ± 1.5 yr, which is 5–13 % lower than recently published observational estimates (Prinn et al., 2005; Prather et al., 2012). Our estimated mean present day tropospheric methyl chloroform lifetime of 5.7 ± 0.9 yr is also about 5–10 % lower than recent observationally-derived estimates (Prinn et al., 2005; Prather et al., 2012), suggesting that the multi-model mean OH is slightly overestimated but is within the range of uncertainties. The models likely overestimate OH abundances in the Northern Hemisphere (NH) versus Southern Hemisphere (SH), as suggested by lower simulated CO

ACPD
12, 30755–30804, 2012

concentrations and higher ozone concentrations (Young et al., 2012) in the NH compared with observations.

We calculated the change in OH and methane lifetime for present day relative to preindustrial and to 1980 to gain a better understanding of their long-term changes. Globally, we find that concurrent increases in the sources of OH (humidity, tropospheric ozone, and NO_x emissions), together with decreases in stratospheric ozone and increase in tropospheric temperature, have been compensated by increases in OH sinks (methane concentration, CO and NMVOC emissions). The net result is a nearly constant global mean OH concentration over the past 150 yr, despite large regional changes, consistent with previous studies (Lelieveld et al., 2002, 2004). Over the same time period, the tropospheric methane lifetime against loss by OH has decreased slightly (-2.0 ± 8.8 %), possibly resulting from a warming-induced increase in its chemical loss. For the 1980 to 2000 period, we find that global mean OH has increased only slightly (3.5 ± 2.2 %) and methane lifetime has decreased by about 4.3 ± 1.9 % in response to this small OH increase and climate warming. The multi-model mean OH change for 1980–2000 disagrees with previous work based on CH_3CCl_3 observations, which suggest a reduction in OH in 2000 relative to 1980 (Prinn et al., 2001; Bousquet et al., 2005), but agrees well with other modelling studies (Karlsdttir and Isaksen, 2000; Dentener et al., 2003; Dalsøren and Isaksen, 2006; John et al., 2012; Holmes et al., 2012) as well as a recent study of OH variability inferred from observations (Montzka et al., 2011).

Substantial intermodel diversity exists in the calculated trends (sign and magnitude) in OH and methane lifetimes for the preindustrial to present day change, stemming from the unique ways the chemical and physical drivers of OH interact within each model. Particularly, we find that the preindustrial to present day OH trend simulated by a model depends on the ratio of the simulated change in CO and NO_x burdens. With a few exceptions, models with high $\Delta CO/\Delta NO_x$ predict OH decreases while those with lower values simulate OH increases from preindustrial to present day (Fig. 3). This relationship reflects the diversity in the chemical schemes implemented as well

ACPD
12, 30755–30804, 2012

as uncertainties in natural CO, NO_x and NMVOC emissions. The representation of the degradation of NMVOC included in models is highly uncertain and better constraints are needed (Archibald et al., 2010; Barkley et al., 2011). For example, several proposed oxidation mechanisms implemented in global chemistry-climate models have yet to satisfactorily explain the model underestimate of OH concentrations observed over dense tropical forests in low-NO_x conditions (e.g., Butler et al., 2008; Lelieveld et al., 2008; Peeters et al., 2009; Paulot et al., 2009; Stavrakou et al., 2010; Barkley et al., 2011).

Using a subset of the models, we further explored the sensitivity of OH and methane lifetime to historical climate change. We find that preindustrial to present day climate change has increased global mean OH and has decreased the methane lifetime by 0.30 ± 0.24 yr, representing a small negative feedback on the climate system. We further attribute preindustrial to present day OH changes to individual increases in methane burden, and anthropogenic emissions of CO, NO_x, and NMVOCs employing additional perturbations simulations from a few models. With fixed methane burden, we find that NO_x emissions increase OH by 46.4 ± 12.2 %, while methane, CO and NMVOCs decrease OH by 17.3 ± 2.3 %, 7.6 ± 1.5 %, and 3.1 ± 3.0 %, respectively. The response of OH and methane lifetime to emission perturbations would be somewhat different if we had allowed methane abundances to respond to these perturbations, lessening the response to NO_x increases but amplifying to methane, CO and NMVOCs increases (Shindell et al., 2005, 2009; Stevenson et al., 2012).

To fully attribute preindustrial to present-day changes in OH, it is necessary to consider changes in other processes that influence OH. Previous studies have shown OH to be sensitive to biogenic NMVOCs (Wu et al., 2007 and references therein), natural (soil + lightning) NO_x emissions (Labrador et al., 2004; Steinkamp et al., 2009), and aerosols (Lamarque et al., 2005b; John et al., 2012, Mao et al., 2012b). For example, future studies with chemistry-climate models should explore how potential climate and land-use driven changes in biogenic NMVOCs (Lathière et al., 2010) and natural NO_x emissions since preindustrial times have impacted the present day OH abundance and

ACPD
12, 30755–30804, 2012

methane lifetime. Furthermore, similar attribution simulations would be helpful in interpreting the influence of each driving factor on OH and methane lifetime since 1980. The role of stratospheric ozone loss in driving OH changes over this period is particularly important (e.g. Dentener et al., 2003).

Overall, we show that the multi-model mean OH abundance has remained nearly constant over the past 150 yr. There is, however, large model-to-model variability in the simulated OH trend, suggesting that a better understanding of the processes influencing atmospheric OH is needed to alleviate uncertainties in its long-term trends and interannual variability (Holmes et al., 2012). We cannot overemphasize the value of accurate observational constraints on OH (e.g. Mao et al., 2012a), either through direct measurements or by indirect methods using proxies, which are needed not only to improve our understanding of OH distributions but also help evaluate the global models.

Supplementary material related to this article is available online at: http://www.atmos-chem-phys-discuss.net/12/30755/2012/acpd-12-30755-2012-supplement.pdf.

Acknowledgements. ACCMIP is organized under the auspices of Atmospheric Chemistry and Climate (AC&C), a project of International Global Atmospheric Chemistry (IGAC) and Stratospheric Processes And their Role in Climate (SPARC) under the International Geosphere-Biosphere Project (IGBP) and World Climate Research Program (WCRP). The authors are grateful to the British Atmospheric Data Centre (BADC), which is part of the NERC National Centre for Atmospheric Science (NCAS), for collecting and archiving the ACCMIP data.

For CESM-CAM-superfast, DB and PC were funded by the US Dept. of Energy (BER), performed under the auspices of LLNL under Contract DE-AC52-07NA27344, and used the supercomputing resources of NERSC under contract No. DE-AC02-05CH11231.

The CICERO-OSloCTM2 simulations were done within the projects SLAC (Short Lived Atmospheric Components) and EarthClim funded by the Norwegian Research Council.

DP would like to thank the Canadian Foundation for Climate and Atmospheric Sciences for their long-running support of CMAM development.

For EMAC, the work of VE and MR was funded by the DLR Earth System Model Validation (ESMVal) project and used the supercomputing resources of the German Climate Computing Center (DKRZ) and the Leibniz Supercomputing Centre (LRZ), and the work of IC was funded by the ENEA National Integrated Model to support the international negotiation on atmospheric pollution (Minni) project.

The GEOSCCM work was supported by the NASA Modeling, Analysis and Prediction program, with computing resources provided by NASA's High-End Computing Program through the NASA Advanced Supercomputing Division.

VN and LWH acknowledge efforts of GFDL's Global Atmospheric Model Development Team in the development of the GFDL-AM3 and Modeling Services Group for assistance with data processing.

AV, DTS and YHL acknowledge support from the NASA MAP and ACMAP programs.

For HadGEM2, WJC, GAF, and STR were supported by the Joint DECC and Defra Integrated Climate Programme (GA01101).

The LMDzORINCA simulations were done using computing resources provided by the CCRT/GENCI computer center of the CEA.

The MIROC-CHEM calculations were performed on the NIES supercomputer system (NEC SX-8R), and supported by the Environment Research and Technology Development Fund (S-7) of the Ministry of the Environment, Japan.

The MOCAGE simulations were supported by Météo-France and CNRS. Supercomputing time was provided by Météo-France/DSI supercomputing center.

The CESM project, including NCAR-CAM3.5, is supported by the National Science Foundation and the Office of Science (BER) of the US Department of Energy. The National Center for Atmospheric Research is operated by the University Corporation for Atmospheric Research under sponsorship of the National Science Foundation.

The STOC-HadAM3 work was supported by cross UK research council grant NE/I008063/1 and used facilities provided by the UK's national high-performance computing service, HECToR, through Computational Modelling Services (CMS), part of the NERC National Centre for Atmospheric Science (NCAS).

ACPD

12, 30755–30804, 2012

The TM5 simulations were performed on the high-performance computing facility of the European Centre for Medium-Range Weather Forecasts (ECMWF).

For UM-CAM, GZ acknowledges NIWA HPCF facility and funding from New Zealand Ministry of Science and Innovation.

We are grateful to Jasmin John and Jingqiu Mao for reviewing an earlier version of this manuscript.

References

Archibald, A. T., Cooke, M. C., Utembe, S. R., Shallcross, D. E., Derwent, R. G., and Jenkin, M. E.: Impacts of mechanistic changes on HO_x formation and recycling in the oxidation of isoprene, Atmos. Chem. Phys., 10, 8097–8118, doi:10.5194/acp-10-8097-2010, 2010.

Barkley, M. P., Palmer, P. I., Ganzeveld, L., Arneth, A., Hågberg, D., Karl, T., Guenther, A., Paulot, F., Wennberg, P. O., Mao, J., Kurosu, T. P., Chance, K., Muller, J.-F., De Smedt, I., Van Roozendael, M., Chen, D., Wang, Y., and Yantosca, R. M.: Can a state of the art chemistry transport model simulate Amazonian tropospheric chemistry?, J. Geophys. Res., 16, D16302, doi:10.1029/2011JD015893, 2011.

Berntsen, T. K., Isaksen, I. S. A., Myhre, G., Fuglestvedt, J. S., Stordal, F., Larsen, T. A., Freckleton, R. S., and Shine, K. P.: Effects of anthropogenic emissions on tropospheric ozone and its radiative forcing, J. Geophys. Res., 102, 28101–28126, doi:10.1029/97JD02226, 1997.

Bousquet, P., Hauglustaine, D. A., Peylin, P., Carouge, C., and Ciais, P.: Two decades of OH variability as inferred by an inversion of atmospheric transport and chemistry of methyl chloroform, Atmos. Chem. Phys., 5, 2635–2656, doi:10.5194/acp-5-2635-2005, 2005.

Bousserez, N., Attié, J. L., Peuch, V. H., Michou, M., Pfister, G., Edwards, D., Emmons, L., Mari, C., Barret, B., Arnold, S. R., Heckel, A., Richert, A., Schlager, H., Lewis, A., Avery, M., Sachse, G., Browell, E. V., and Hair, J. W.: Evaluation of the MOCAGE chemistry transport model during the ICARTT/ITOP experiment, J. Geophys., Res., 112, D10S42, doi:10.1029/2006JD007595, 2007.

Bowman, K., Shindell, D., Worden, H., Lamarque, J. F., Young, P. J., Stevenson, D., Qu, Z., de la Torre, M., Bergmann, D., Cameron-Smith, P., Collins, W. J., Doherty, R., Dalsøren, S., Faluvegi, G., Folberth, G., Horowitz, L. W., Josse, B., Lee, Y. H., MacKenzie, I., Myhre, G.,

ACPD

12, 30755–30804, 2012

Nagashima, T., Naik, V., Plummer, D., Rumbold, S., Skeie, R., Strode, S., Sudo, K., Szopa, S., Voulgarakis, A., Zeng, G., Kulawik, S., and Worden, J.: Observational constraints on ozone radiative forcing from the Atmospheric Chemistry Climate Model Intercomparison Project (ACCMIP), Atmos. Chem. Phys. Discuss., 12, 23603–23644, doi:10.5194/acpd-12-23603-2012, 2012.

Butler, T. M., Taraborrelli, D., Brühl, C., Fischer, H., Harder, H., Martinez, M., Williams, J., Lawrence, M. G., and Lelieveld, J.: Improved simulation of isoprene oxidation chemistry with the ECHAM5/MESSy chemistry-climate model: lessons from the GABRIEL airborne field campaign, Atmos. Chem. Phys., 8, 4529—4546, doi:10.5194/acp-8-4529-2008, 2008.

Crutzen, P. J.: A discussion of the chemistry of some minor constituents in the stratosphere and troposphere, Pure Appl. Geophys., 106–108, 1385–1399, 1973.

Crutzen, P. J. and Brühl, C.: A model study of atmospheric temperatures and the concentrations of ozone, hydroxyl, and some other photochemically active gases during the glacial, the pre-industrial, Holocene, and the present, Geophys. Res. Lett., 20, 1047–1050, 1993.

Dalsøren, S. B. and Isaksen, I. S. A.: CTM study of changes in tropospheric hydroxyl distribution 1990–2001 and its impact on methane, Geophys. Res. Lett., 33, L23811, doi:10.1029/2006GL027295, 2006.

Deeter, M. N., Edwards, D. P., Gille, J. C., Emmons, L. K., Francis, G., Ho, S.-P., Mao, D., Masters, D., Worden, H., Drummond, J. R., and Novelli, P. C.: The MOPITT version 4 CO product: algorithm enhancements, validation, and long-term stability, J. Geophys. Res., 115, D07306, doi:10.1029/2009JD013005, 2010.

Dentener, F., Peters, W., Krol, M., Van Weele, M., Bergamaschi, P., and Lelieveld, J.: Interannual variability and trend of CH_4 lifetime as a measure for OH changes in the 1979–1993 time period, J. Geophys. Res., 108, 4442, doi:10.1029/2002JD002916, 2003.

Derwent, R. G., Collins, W. J., Johnson, C. E., and Stevenson, D. S.: Transient behaviour of tropospheric ozone precursors in a global 3-D CTM and their indirect greenhouse effects, Clim. Change, 49, 463–487, 2001.

Emmons, L. K., Edwards, D. P., Deeter, M. N., Gille, J. C., Campos, T., Nédélec, P., Novelli, P., and Sachse, G.: Measurements of Pollution In The Troposphere (MOPITT) validation through 2006, Atmos. Chem. Phys., 9, 1795–1803, doi:10.5194/acp-9-1795-2009, 2009.

Fiore, A. M., West, J. J., Horowitz, L. W., Naik, V., and Schwarzkopf, M. D.: Characterizing the tropospheric ozone response to methane emission controls and the benefits to climate and air quality, J. Geophys. Res., 113, D08307, doi:10.1029/2007JD009162, 2008.

ACPD
12, 30755–30804, 2012

Fiore, A. M., Dentener, F. J., Wild, O., Cuvelier, C., Schultz, M. G., Hess, P., Textor, C., Schulz, M., Doherty, R. M., Horowitz, L. W., MacKenzie, I. A., Sanderson, M. G., Shindell, D. T., Stevenson, D. S., Szopa, S., Van Dingenen, R., Zeng, G., Atherton, C., Bergmann, D., Bey, I., Carmichael, G., Collins, W. J., Duncan, B. N., Faluvegi, G., Folberth, G., Gauss, M., Gong, S., Hauglustaine, D., Holloway, T., Isaksen, I. S. A., Jacob, D. J., Jonson, J. E., Kaminski, J. W., Keating, T. J., Lupu, A., Marmer, E., Montanaro, V., Park, R. J., Pitari, G., Pringle, K. J., Pyle, J. A., Schroeder, S., Vivanco, M. G., Wind, P., Wojcik, G., Wu, S., and Zuber, A.: Multimodel estimates of intercontinental source-receptor relationships for ozone pollution, J. Geophys. Res., 114, D04301, doi:10.1029/2008JD010816, 2009.

Granier, C., Bessagnet, B., Bond, T., D'Angiola, A., v. d. Gon, H. D., Frost, G. J., Heil, A., Kaiser, J. W., Kinne, S., Klimont, Z., Kloster, S., Lamarque, J.-F., Liousse, C., Masui, T., Meleux, F., Mieville, A., Ohara, T., Raut, J.-C., Riahi, K., Schultz, M. G., Smith, S. J., Thomson, A., van Aardenne, J., van der Werf, G. R., and van Vuuren, D. P.: Evolution of anthropogenic and biomass burning emissions of air pollutants at global and regional scales during the 1980–2010 period, Clim. Change, 109, 163–190, doi:10.1007/s10584-011-0154-1, 2011.

Grenfell, J. L., Shindell, D. T., Koch, D., and Rind, D.: Chemistry-climate interactions in the Goddard Institute general circulation model, 2: New insights into modeling the pre-industrial atmosphere, J. Geophys. Res., 106, 33435–33451, 2001.

Hameed, S., Pinto, J. P., and Stewart, R. W.: Sensitivity of the predicted CO–OH–CH_4 perturbation to tropospheric NO_x concentrations, J. Geophys. Res., 84, 763–768, 1979.

Hauglustaine, D. A. and Brasseur, G. P.: Evolution of tropospheric ozone under anthropogenic activities and associated radiative forcing of climate, J. Geophys. Res., 106, 32337–32360, doi:10.1029/2001JD900175, 2001.

Holmes, C. D., Prather, M. J., Søvde, O. A., and Myhre, G.: Future methane, hydroxyl, and their uncertainties: key climate and emission parameters for future predictions, Atmos. Chem. Phys. Discuss., 12, 20931–20974, doi:10.5194/acpd-12-20931-2012, 2012.

Jacob, D. J.: Introduction to Atmospheric Chemistry, Princeton University Press, Princeton, New Jersey, USA, 1999.

John, J. G., Fiore, A. M., Naik, V., Horowitz, L. W., and Dunne, J. P.: Climate versus emission drivers of methane lifetime from 1860–2100, Atmos. Chem. Phys. Discuss., 12, 18067–18105, doi:10.5194/acpd-12-18067-2012, 2012.

ACPD
12, 30755–30804, 2012

Johnson, C. E., Stevenson, D. S., Collins, W. J., and Derwent, R. G.: Role of climate feedback on methane and ozone studies with a coupled ocean-atmosphere-chemistry model, Geophys. Res. Lett., 28, 1723–1726, 2001.
Karlsdóttir, S. and Isaksen, I. S. A.: Changing methane lifetime – possible cause for reduced growth, Geophys. Res. Lett., 27, 93–96, 2000.
Krol, M. and Lelieveld, J.: Can the variability in tropospheric OH be deduced from measurements of 1,1,1-trichloroethane (methyl chloroform)?, J. Geophys. Res., 108, 4125, doi:10.1029/2002JD002423, 2003.
Krol, M., van Leeuwen, P. J., and Lelieveld, J.: Global OH trend inferred from methyl-3 chloroform measurements, J. Geophys. Res., 103, 10697–10711, 1998.
Labrador, L. J., von Kuhlmann, R., and Lawrence, M. G.: Strong sensitivity of the global mean OH concentration and the tropospheric oxidizing efficiency to the source of NO_x from lightning, Geophys. Res. Lett., 31, L06102, doi:10.1029/2003GL019229, 2004.
Lamarque, J.-F., Hess, P., Emmons, L. K., Buja, L., Washington, W., and Granier, C.: Tropospheric ozone evolution between 1890 and 1990, J. Geophys. Res., 110, D08304, doi:10.1029/2004JD005537, 2005a.
Lamarque, J.-F., Kiehl, J. T., Hess, P. G., Collins, W. D., Emmons, L. K., Ginoux, P., Luo, C., and Tie, X. X.: Response of a coupled chemistry-climate model to changes in aerosol emissions: global impact on the hydrological cycle and the tropospheric burden of OH, ozone, and NO_x, Geophys. Res. Lett., 32, L16809, doi:10.1029/2005GL023419, 2005b.
Lamarque, J.-F., Bond, T. C., Eyring, V., Granier, C., Heil, A., Klimont, Z., Lee, D., Liousse, C., Mieville, A., Owen, B., Schultz, M. G., Shindell, D., Smith, S. J., Stehfest, E., Van Aardenne, J., Cooper, O. R., Kainuma, M., Mahowald, N., McConnell, J. R., Naik, V., Riahi, K., and van Vuuren, D. P.: Historical (1850–2000) gridded anthropogenic and biomass burning emissions of reactive gases and aerosols: methodology and application, Atmos. Chem. Phys., 10, 7017–7039, doi:10.5194/acp-10-7017-2010, 2010.
Lamarque, J.-F., Shindell, D. T., Josse, B., Young, P. J., Cionni, I., Eyring, V., Bergmann, D., Cameron-Smith, P., Collins, W. J., Doherty, R., Dalsoren, S., Faluvegi, G., Folberth, G., Ghan, S. J., Horowitz, L. W., Lee, Y. H., MacKenzie, I. A., Nagashima, T., Naik, V., Plummer, D., Righi, M., Rumbold, S., Schulz, M., Skeie, R. B., Stevenson, D. S., Strode, S., Sudo, K., Szopa, S., Voulgarakis, A., and Zeng, G.: The Atmospheric Chemistry and Climate Model Intercomparison Project (ACCMIP): overview and description of models, simulations

ACPD
12, 30755–30804, 2012

and climate diagnostics, Geosci. Model Dev. Discuss., 5, 2445–2502, doi:10.5194/gmdd-5-2445-2012, 2012.
Lathière, J., Hewitt, C. N., and Beerling, D. J.: Sensitivity of isoprene emissions from the terrestrial biosphere to 20th century changes in atmospheric CO_2 concentration, climate, and land use, Global Biogeochem. Cy., 24, GB1004, doi:10.1029/2009GB003548, 2010.
Lawrence, M. G., Jöckel, P., and von Kuhlmann, R.: What does the global mean OH concentration tell us?, Atmos. Chem. Phys., 1, 37–49, doi:10.5194/acp-1-37-2001, 2001.
Lee, Y. H., Lamarque, J.-F., Flanner, M. G., Jiao, C., Shindell, D. T., Berntsen, T., Bisiaux, M. M., Cao, J., Collins, W. J., Curran, M., Edwards, R., Faluvegi, G., Ghan, S., Horowitz, L. W., McConnell, J. R., Myhre, G., Nagashima, T., Naik, V., Rumbold, S. T., Skeie, R. B., Sudo, K., Takemura, T., and Thevenon, F.: Evaluation of preindustrial to present-day black carbon and its albedo forcing from ACCMIP (Atmospheric Chemistry and Climate Model Intercomparison Project), Atmos. Chem. Phys. Discuss., 12, 21713–21778, doi:10.5194/acpd-12-21713-2012, 2012.
Leibensperger, E. M., Mickley, L. J., Jacob, D. J., and Barrett, S. R. H.: Intercontinental influence of NO_x and CO emissions on particulate matter air quality, Atmos. Environ, 45, 3318–3324, 2011.
Lelieveld, J., Peters, W., Dentener, F. J., and Krol, M. C.: Stability of tropospheric hydroxyl chemistry, J. Geophys. Res., 107, 4715, doi:10.1029/2002JD002272, 2002.
Lelieveld, J., Dentener, F. J., Peters, W., and Krol, M. C.: On the role of hydroxyl radicals in the self-cleansing capacity of the troposphere, Atmos. Chem. Phys., 4, 2337–2344, doi:10.5194/acp-4-2337-2004, 2004.
Lelieveld, J., Butler, T. M., Crowley, J. N., Dillon, T. J., Fischer, H., Ganzeveld, L., Harder, H., Lawrence, M. G., Martinez, M., Taraborrelli, D., and Williams, J.: Atmospheric oxidation capacity sustained by a tropical forest, Nature, 452, 737–740, doi:10.1038/nature06870, 2008.
Levy, H.: Normal atmosphere: large radical and formaldehyde concentrations predicted, Science, 173, 141–143, 1971.
Logan, J. A., Prather, M. J., Wofsy, S. C., and McElroy, M. B.: Tropospheric chemistry: a global perspective, J. Geophys. Res., 86, 7210–7354, 1981.
Loulergue, L., Schilt, A., Spahni, R., Masson-Delmotte, V., Blunier, T., Benedicte, L., Barnola, J.-M., Raynaud, D., Stocker, T. F., and Chappellaz, J.: Orbital and millennial-scale features of atmospheric CH_4 over the past 800 000 years, Nature 453, 383–386, 2008.

ACPD
12, 30755–30804, 2012

Martinerie, P., Brasseur, G. P., and Granier, C.: The chemical composition of ancient atmospheres: a model study constrained by ice core data, J. Geophys. Res., 100, 14291–14304, 1995.

Mao, J., Ren, X., Zhang, L., Van Duin, D. M., Cohen, R. C., Park, J.-H., Goldstein, A. H., Paulot, F., Beaver, M. R., Crounse, J. D., Wennberg, P. O., DiGangi, J. P., Henry, S. B., Keutsch, F. N., Park, C., Schade, G. W., Wolfe, G. M., Thornton, J. A., and Brune, W. H.: Insights into hydroxyl measurements and atmospheric oxidation in a California forest, Atmos. Chem. Phys., 12, 8009–8020, doi:10.5194/acp-12-8009-2012, 2012a.

Mao, J., Fan, S., Jacob, D. J., and Travis, K. R.: Radical loss in the atmosphere from Cu-Fe redox coupling in aerosols, Atmos. Chem. Phys. Discuss., 12, 27053–27076, doi:10.5194/acpd-12-27053-2012, 2012b.

Meinshausen, M., Smith, S. J., Calvin, K. V., Daniel, J. S., Kainuma, M., Lamarque, J.-F., Matsumoto, K., Montzka, S. A., Raper, S. C. B., Riahi, K., Thomson, A. M., Velders, G. J. M., and van Vuuren D.: The RCP greenhouse gas concentrations and their extension from 1765 to 2300, Clim. Change, 109, 213–241, doi:10.1007/s10584-011-0156-z, 2011.

Mickley, L. J., Murti, P. P., Jacob, D. J., Logan, J. A., Koch, D. M., and Rind, D.: Radiative forcing from tropospheric ozone calculated with a unified chemistry climate model, J. Geophys. Res., 104, 30153–30172, 1999.

Monteil, G., Houweling, S., Dlugockenky, E. J., Maenhout, G., Vaughn, B. H., White, J. W. C., and Rockmann, T.: Interpreting methane variations in the past two decades using measurements of CH_4 mixing ratio and isotopic composition, Atmos. Chem. Phys., 11, 9141–9153, doi:10.5194/acp-11-9141-2011, 2011.

Montzka, S. A. and Fraser, P. J.: Controlled substances and other source gases, in: Scientific Assessment of Ozone Depletion: 2002, Global Ozone Res. and Monitor. Proj. Rep. 47, chap. 1, World Meteorol. Organ., Geneva, Switzerland, 498 pp., 2003.

Montzka, S. A., Spivakovsky, C. M., Butler, J. H., Elkins, J. W., Lock, L. T., and Mondeel, D. J.: New observational constraints, for atmospheric hydroxyl on global and hemispheric scales, Science, 288, 500–503, 2000.

Montzka, S. A., Krol, M., Dlugokencky, E., Hall, B., Jöckel, P., and Lelieveld, J.: Small 21 interannual variability of global atmospheric hydroxyl, Science, 331, 67–69, doi:10.1126/science.1197640, 2011.

ACPD
12, 30755–30804, 2012

Naik, V., Mauzerall, D., Horowitz, L. W., Schwarzkopf, D., Ramaswamy, V., and Oppenheimer, M.: Net radiative forcing due to changes in regional emissions of tropospheric ozone precursors, J. Geophys. Res., 110, D24306, doi:10.1029/2005JD005908, 2005.

Novelli, P. C. and Masarie, K. A.: Atmospheric Carbon Monoxide Dry Air Mole Fractions from the NOAA ESRL Carbon Cycle Cooperative Global Air Sampling Network, 1988–2009, Version: 2011-10-14, available at: ftp://ftp.cmdl.noaa.gov/ccg/co/flask/event/, downloaded on 11 April 2012, 2010.

Paulot, F., Crounse, J. D., Kjaergaard, H. G., Kurten, A., St. Clair, J. M., Seinfeld, J. H., and Wennberg, P. O.: Unexpected epoxide formation in the gas-phase photooxidation of isoprene, Science, 325, 730–733, doi:10.1126/science.1172910, 2009.

Peeters, J., Nguyen, T. L., and Vereecken, L.: HO_x radical regeneration in the oxidation of isoprene, Phys. Chem. Chem. Phys., 11, 5935–5939, doi:10.1039/b908511d, 2009.

Petit, J. R., Jouzel, J., Raynaud, D., Barkov, N. I., Barnola, J.-M., Basile, I., Bender, M., Chappellaz, J., Davis, M., Delaygue, G., Delmotte, M., Kotlaykov, V. M., Legrand, M., Lipenkov, V. Y., Lorius, C., Pepin, L., Ritz, C., Saltzman, E., and Stievenard, M.: Climate and atmospheric history of the past 420 000 years from the Vostock ice core, Antarctica, Nature, 399, 429–436, 1999.

Pinto, J. P. and Khalil, M. A. K.: The stability of tropospheric OH during ice gases, interglacial epochs and modern times, Tellus, 43B, 347–352, 1991.

Prather, M. J.: Lifetimes and eigenstates in atmospheric chemistry, Geophys. Res. Lett. 21, 801–804, 1994.

Prather, M. J.: Time scales in atmospheric chemistry: Theory, GWPs for CH_4 and CO, and runaway growth, Geophys. Res. Lett., 23, 2597–2600, 1996.

Prather, M. and Spivakovsky, C. M.: Tropospheric OH and the lifetimes of hydrochlorofluorocarbons, J. Geophys. Res., 95, 18723–18729, doi:10.1029/JD095iD11p18723, 1990.

Prather, M., Ehhalt, D., Dentener, F., Derwent, R. G., Dlugokencky, E., Holland, E., Isaksen, I. S. A., Katima, J., Kirchhoff, V., Matson, P., Midgley, P. M. and Wang, M.: Atmospheric chemistry and greenhouse gases, in: Climate Change 2001: The Scientific Basis, Chap. 4, edited by: Houghton, J. T. et al., Cambridge University Press, Cambridge, UK, 239–287, 2001.

Prather, M., Holmes, C., and Hsu, J.: Reactive greenhouse gas scenarios: systematic exploration of uncertainties and the role of atmospheric chemistry, Geophys. Res. Lett., 39, L09803, doi:10.1029/2012GL051440, 2012.

ACPD
12, 30755–30804, 2012

Prinn, R. G., Weiss, R. F., Miller, B. R., Huang, J., Alyea F. N., Cunnold, D. M., Fraser, P. J., Hartley, D. E., and Simmonds, P. G.: Atmospheric trends and lifetime of CH_3CCl_3 and global OH concentrations, Science, 269, 187–192, 1995.

Prinn, R. G., Weiss, R. F., Fraser, P. J., Simmonds, P. G., Cunnold, D. M., Alyea, F. N., O'Doherty, S., Salameh, P., Miller, B. R., Huang, J., Wang, R. H. J., Hartley, D. E., Harth, C., Steele, L. P., Sturrock, G., Midgley, P. M., and McCulloch, A.: A history of chemically and radiatively important gases in air deduced from ALE/GAGE/AGAG E, J. Geophys. Res., 105, 17751–17792, 2000.

Prinn, R. G., Huang, J., Weiss, R. F., Cunnold, D. M., Fraser, P. J., Simmonds, P. G., McCulloch, A., Harth, C., Salameh, P., O'Doherty, S., Wang, R. H. J., Porter, L., and Miller, B. R.: Evidence for substantial variations of atmospheric hydroxyl radicals over the past two 21 decades, Science, 292, 1882–1888, 2001.

Prinn, R. G., Huang, J., Weiss, R. F., Cunnold, D. M., Fraser, P. J., Simmonds, P. G., McCulloch, A., Harth, C., Reimann, S., Salameh, P., O'Doherty, S., Wang, R. H. J., Porter, L. W., Miller, B. R., and Krummel, P. B.: Evidence for variability of atmospheric hydroxyl radicals over the past quarter century, Geophys. Res. Lett., 32, L07809, doi:10.1029/2004GL022228, 2005.

Sander, S. P., Abbatt, J., Barker, J. R., Burkholder, J. B., Friedl, R. R., Golden, D. M., Huie, R. E., Kolb, C. E., Kurylo, M. J., Moortgat, G. K., Orkin, V. L., Wine, P. H.: Chemical kinetics and photochemical data for use in atmospheric studies: evaluation number 17, JPL Publication 10-6, Jet Propulsion Laboratory, Pasadena, 2011.

Sapart, S. J., Monteil, G., Prokopiou, M., van de Wal, R. S. W., Kaplan, J. O., Sperlich, P., Krumhardt, K. M., van der Veen, C., Houweling, S., Krol, M. C., Blunier, T., Sowers, T., Martinerie, P., Witrant, E., Dahl-Jensen, D., and Röckmann, T.: Natural and anthropogenic variations in methane sources during the past two millennia, Nature, 490, 85–88, doi:10.1038/nature11461, 2012.

Shindell, D. T., Faluvegi, G., and Bell, N.: Preindustrial-to-present-day radiative forcing by tropospheric ozone from improved simulations with the GISS chemistry-climate GCM, Atmos. Chem. Phys., 3, 1675–1702, doi:10.5194/acp-3-1675-2003, 2003.

Shindell, D. T., Faluvegi, G., Bell, N., and Schmidt, G. A.: An emissions-based view of climate forcing by methane and tropospheric ozone, Geophys. Res. Lett., 32, L04803, doi:10.1029/2004GL021900, 2005.

ACPD
12, 30755–30804, 2012

Shindell, D. T., Faluvegi, G., Unger, N., Aguilar, E., Schmidt, G. A., Koch, D. M., Bauer, S. E., and Miller, R. L.: Simulations of preindustrial, present-day, and 2100 conditions in the NASA GISS composition and climate model G-PUCCINI, Atmos. Chem. Phys., 6, 4427–4459, doi:10.5194/acp-6-4427-2006, 2006a.

Shindell, D. T., Faluvegi, G., Stevenson, D. S., Krol, M. C., Emmons, L. K., Lamarque, J.-F., Petron, G., Dentener, F. J., Ellingsen, K., Schultz, M. G., Wild, O., Amann, M., Atherton, C. S., Bergmann, D. J., Bey, I., Butler, T., Cofala, J., Collins, W. J., Derwent, R. G., Doherty, R. M., Drevet, J., Eskes, H. J., Fiore, A. M., Gauss, M., Hauglustaine, D. A., Horowitz, L. W., Isaksen, I. S. A., Lawrence, M. G., Montanaro, V., Müller, J.-F., Pitari, G., Prather, M. J., Pyle, J. A., Rast, S., Rodriguez, J. M., Sanderson, M. G., Savage, N. H., Strahan, S. E., Sudo, K., Szopa, S., Unger, N., van Noije, T. P. C., and Zeng, G: Multimodel simulations of carbon monoxide: comparison with observations and projected near-future changes, J. Geophys. Res., 111, D19306, doi:10.1029/2006JD007100, 2006b.

Shindell, D. T., Faluvegi, Koch, D. M., Schmidt, G. A., Unger, N., and Bauer, S. E.: Improved attribution of climate forcing to emissions, Science, 326, 716–718, doi:10.1126/science.1174760, 2009.

Shindell, D. T., Lamarque, J.-F., Schulz, M., Flanner, M., Jiao, C., Chin, M., Young, P., Lee, Y. H., Rotstayn, L., Milly, G., Faluvegi, G., Balkanski, Y., Collins, W. J., Conley, A. J., Dalsoren, S., Easter, R., Ghan, S., Horowitz, L., Liu, X., Myhre, G., Nagashima, T., Naik, V., Rumbold, S., Skeie, R., Sudo, K., Szopa, S., Takemura, T., Voulgarakis, A., and Yoon, J.-H.: Radiative forcing in the ACCMIP historical and future climate simulations, Atmos. Chem. Phys. Discuss., 12, 21105–21210, doi:10.5194/acpd-12-21105-2012, 2012.

Skeie, R. B., Berntsen, T. K., Myhre, G., Tanaka, K., Kvalevåg, M. M., and Hoyle, C. R.: Anthropogenic radiative forcing time series from pre-industrial times until 2010, Atmos. Chem. Phys., 11, 11827–11857, doi:10.5194/acp-11-11827-2011, 2011.

Sofen, E. D., Alexander, B., and Kunasek, S. A.: The impact of anthropogenic emissions on atmospheric sulfate production pathways, oxidants, and ice core $\Delta^{17}O(SO_4^{2-})$, Atmos. Chem. Phys., 11, 3565–3578, doi:10.5194/acp-11-3565-2011, 2011.

Spivakovsky, C. M., Logan, J. A., Montzka, S. A., Balkanski, Y. J., Foreman-Fowler, M., Jones, D. B. A., Horowitz, L. W., Fusco, A. C., Brenninkmeijer, C. A. M., Prather, M. J., Wofsy, S. C., and McElroy, M. B.: Three-dimensional climatological distribution of tropospheric OH: update and evaluation, J. Geophys. Res., 105, 8931–8980, 2000.

ACPD
12, 30755–30804, 2012

Staffelbach, T., Neftel, A., Stauffer, B., and Jacob, D.: A record of the atmospheric methane sink from formaldehyde in polar ice cores, Nature, 349, 603–605, doi:10.1038/349603a0, 1991.
Stavrakou, T., Peeters, J., and Müller, J.-F.: Improved global modelling of HO_x recycling in isoprene oxidation: evaluation against the GABRIEL and INTEX-A aircraft campaign measurements, Atmos. Chem. Phys., 10, 9863–9878, doi:10.5194/acp-10-9863-2010, 2010.
Steinkamp, J., Ganzeveld, L. N., Wilcke, W., and Lawrence, M. G.: Influence of modelled soil biogenic NO emissions on related trace gases and the atmospheric oxidizing efficiency, Atmos. Chem. Phys., 9, 2663–2677, doi:10.5194/acp-9-2663-2009, 2009.
Stevenson, D. S., Johnson, C. E., Collins, W. J., Derwent, R. G., and Edwards, J. M.: Future tropospheric ozone radiative forcing and methane turnover – the impact of climate change, Geophys. Res. Lett. 27, 2073–2076, 2000.
Stevenson, D. S., Doherty, R. M., Sanderson, M. G., Collins, W. J., Johnson, C. E., and Derwent, R. G.: Radiative forcing from aircraft NO_x emissions: mechanisms and seasonal dependence, J. Geophys. Res., 109, D17307, doi:10.1029/2004JD004759, 2004.
Stevenson, D. S., Dentener, F. J., Schultz, M. G., Ellingsen, K., van Noije, T. P. C., Wild, O., Zeng, G., Amann, M., Atherton, C. S., Bell, N., Bergmann, D. J., Bey, I., Butler, T., Cofala, J., Collins, W. J., Derwent, R. G., Doherty, R. M., Drevet, J., Eskes, H. J., Fiore, A. M., Gauss, M., Hauglustaine, D. A., Horowitz, L. W., Isaksen, I. S. A., Krol, M. C., Lamarque, J., Lawrence, M. G., Montanaro, V., Müller, J., Pitari, G., Prather, M. J., Pyle, J. A., Rast, S., Rodriguez, J. M., Sanderson, M. G., Savage, N. H., Shindell, D. T., Strahan, S. E., Sudo, K., and Szopa, S.: Multimodel ensemble simulations of present day and near-future tropospheric ozone, J. Geophys. Res., 111, D08301, doi:10.1029/2005JD006338, 2006.
Stevenson, D. S., Young, P. J., Naik, V., Lamarque, J.-F., Shindell, D. T., Voulgarakis, A., Skeie, R. B., Dalsoren, S. B., Myhre, G., Berntsen, T. K., Folberth, G. A., Rumbold, S. T., Collins, W. J., MacKenzie, I. A., Doherty, R. M., Zeng, G., van Noije, T. P. C., Strunk, A., Bergmann, D., Cameron-Smith, P., Plummer, D. A., Strode, S. A., Horowitz, L., Lee, Y. H., Szopa, S., Sudo, K., Nagashima, T., Josse, B., Cionni, I., Righi, M., Eyring, V., Conley, A., Bowman, K. W., and Wild, O.: Tropospheric ozone changes, radiative forcing and attribution to emissions in the Atmospheric Chemistry and Climate Model Inter-comparison Project (ACCMIP), Atmos. Chem. Phys. Discuss., 12, 26047–26097, doi:10.5194/acpd-12-26047-2012, 2012.
Thompson, A. M.: The oxidizing capacity of the Earth's atmosphere: probable past and future changes, Science, 256, 1157–1165, 1992.

ACPD
12, 30755–30804, 2012

Voulgarakis, A., Naik, V., Lamarque, J.-F., Shindell, D. T., Young, P. J., Prather, M. J., Wild, O., Field, R. D., Bergmann, D., Cameron-Smith, P., Cionni, I., Collins, W. J., Dalsøren, S. B., Doherty, R. M., Eyring, V., Faluvegi, G., Folberth, G. A., Horowitz, L. W., Josse, B., McKenzie, I. A., Nagashima, T., Plummer, D. A., Righi, M., Rumbold, S. T., Stevenson, D. S., Strode, S. A., Sudo, K., Szopa, S., and Zeng, G.: Analysis of present day and future OH and methane lifetime in the ACCMIP simulations, Atmos. Chem. Phys. Discuss., 12, 22945–23005, doi:10.5194/acpd-12-22945-2012, 2012.

Wang, Y. and Jacob, J. D.: Anthropogenic forcing on tropospheric ozone and OH since preindustrial times, J. Geophys. Res., 103, 31123–31135, 1998.

West, J. J., Fiore, A. M., Naik, V., Horowitz, L. W., Schwarzkopf, M. D., and Mauzerall, D. L.: Ozone air quality and radiative forcing consequences of changes in ozone precursor emissions, Geophys. Res. Lett., 34, L06806, doi:10.1029/2006GL029173, 2007.

Wild, O., Prather M. J., and Akimoto, H., Indirect long-term global cooling from NO_x emissions, Geophys. Res. Lett., 28, 1719–1722, 2001.

Wong, S., Wang, W.-C., Isaksen, I. S. A., Berntsen, T. K., and Sundet, J. K.: A global climate-chemistry model study of present day tropospheric chemistry and radiative forcing from changes in tropospheric O_3 since the preindustrial period, J. Geophys. Res., 109, D11309, doi:10.1029/2003JD003998, 2004.

Wu, S., Mickley, L. J., Jacob, D. J., Logan, J. A., Yantosca, R. M., and Rind, D.: Why are there large differences between models in global budgets of tropospheric ozone?, J. Geophys. Res., 112, D05302, doi:10.1029/2006JD007801, 2007.

Young, P. J., Archibald, A. T., Bowman, K. W., Lamarque, J.-F., Naik, V., Stevenson, D. S., Tilmes, S., Voulgarakis, A., Wild, O., Bergmann, D., Cameron-Smith, P., Cionni, I., Collins, W. J., Dalsøren, S. B., Doherty, R. M., Eyring, V., Faluvegi, G., Horowitz, L. W., Josse, B., Lee, Y. H., MacKenzie, I. A., Nagashima, T., Plummer, D. A., Righi, M., Rumbold, S. T., Skeie, R. B., Shindell, D. T., Strode, S. A., Sudo, K., Szopa, S., and Zeng, G.: Pre-industrial to end 21st century projections of tropospheric ozone from the Atmospheric Chemistry and Climate Model Intercomparison Project (ACCMIP), Atmos. Chem. Phys. Discuss., 12, 21615–21677, doi:10.5194/acpd-12-21615-2012, 2012.

Zimmerman, P. R., Chatfield, R. B., Fishman, J., Crutzen, P. J., and Hanst, P. L.: Estimates of the production of CO and H_2 from the oxidation of hydrocarbon emissions from vegetation, Geophys. Res. Lett., 5, 679–682, 1978.

ACPD
12, 30755–30804, 2012

Table 1. Global total methane burden, airmass-weighted tropospheric mean OH, and tropospheric methane lifetime (τ_{CH_4}) for 1850, 1980 and 2000 time-slices and tropospheric CH_3CCl_3 lifetime (τ_{MCF}) for 2000 time-slice from 16 models. The troposphere is assumed to extend from surface to 200 hPa for each model's grid. A cell with *** means that the model did not report that quantity. Multi-model mean (MMM) with standard deviation (STD) and coefficient of variation (CV) are shown in the last two rows. Models with decreasing methane lifetime over the 1850–2000 period are shown in bold (see Sect. 3).

	CH_4 Burden (Tg)			OH (10^5 molec cm^{-3})			τ_{CH_4} (yr)			τ_{MCF} (yr)
Models	1850	1980	2000	1850	1980	2000	1850	1980	2000	2000
CESM-CAM-superfast (CE)	**2191**	**4431**	**4902**	**12.1**	**12.3**	**12.8**	**9.3**	**8.8**	**8.4**	**4.9**
CICERO-OsloCTM2 (CI)	2089	4286	4779	11.7	10.3	10.4	9.1	10.1	10.0	5.8
CMAM (CM)	2179	4260	4846	11.9	10.6	10.7	8.7	9.7	9.4	5.5
EMAC (EM)	2163	4235	4788	12.7	11.3	11.7	8.9	9.6	9.1	5.4
GEOSCCM (GE)	2178	4258	4818	13.0	11.3	11.3	8.6	9.7	9.6	5.6
GFDL-AM3 (GF)	2221	4234	4809	12.7	11.4	11.7	8.9	9.7	9.4	5.5
GISS-E2-R (GI)	**2188**	**4226**	**4793**	**9.8**	**9.9**	**10.5**	**11.9**	**11.4**	**10.6**	**6.2**
GISS-E2-R-TOMAS (GT)	**2189**	**4499**	**4816**	**11.6**	**12.0**	**12.7**	**10.4**	**9.8**	**9.2**	**5.3**
HadGEM2 (HA)	2155	4133	4680	8.1	7.8	8.1	11.6	12.1	11.6	6.7
LMDzORINCA (LM)	2293	4506	4980	11.0	10.2	10.3	10.1	10.7	10.5	6.1
MIROC-CHEM (MI)	***	***	4805	13.4	12.4	12.4	***	***	8.7	5.1
MOCAGE (MO)	**2126**	**4205**	**4678**	**11.6**	**12.5**	**13.3**	**8.2**	**7.5**	**7.1**	**4.1**
NCAR-CAM3.5 (NC)	**2209**	**4309**	**4903**	**10.7**	**11.3**	**12.0**	**10.7**	**9.9**	**9.2**	**5.4**
STOC-HadAM3 (ST)	2127	4161	4708	11.8	11.6	12.1	9.7	9.6	9.1	5.3
TM5 (TM)	2173	***	4820	10.9	***	10.5	9.8	***	9.9	5.8
UM-CAM (UM)	**2209**	**4323**	**4879**	**7.0**	**7.1**	**7.4**	**15.0**	**14.7**	**14.0**	**8.4**
MMM ± STD	2179 ± 47	42.0 ± 1.5	4813 ± 81	11.3 ± 1.7	10.8 ± 1.6	11.1 ± 1.6	10.1 ± 1.7	10.2 ± 1.7	9.7 ± 1.5	5.7 ± 0.9
CV	0.02	0.03	0.02	0.15	0.15	0.15	0.17	0.16	0.16	0.16

ACPD
12, 30755–30804, 2012

Table 2. Inter-hemispheric ratio (N/S) of tropospheric mean OH from models for 1850, 1980 and 2000 time-slices. Observation-derived estimates shown in the last row are based on Montzka et al. (2001), Prinn et al. (2001), Krol and Lelieveld (2003), and Bousquet et al. (2005).

	N/S Ratio		
Models	1850	1980	2000
CESM-CAM-superfast	1.26	1.40	1.42
CICERO-OsloCTM2	1.22	1.36	1.42
CMAM	1.08	1.16	1.20
EMAC	1.06	1.11	1.13
GEOSCCM	1.07	1.12	1.18
GFDL-AM3	1.07	1.16	1.20
GISS-E2-R	1.01	1.30	1.23
GISS-E2-R-TOMAS	1.02	1.13	1.13
HadGEM2	1.11	1.29	1.34
LMDzORINCA	1.13	1.22	1.24
MIROC-CHEM	1.20	1.27	1.29
MOCAGE	1.03	1.28	1.32
NCAR-CAM3.5	1.29	1.36	1.39
STOC-HadAM3	1.14	1.26	1.31
TM5	1.14	***	1.28
UM-CAM	1.21	1.34	1.40
MMM ± STD	1.13 ± 0.09	1.25 ± 0.10	1.28 ± 0.10
CV	0.08	0.08	0.08
Observation-derived			0.85–0.98

ACPD
12, 30755–30804, 2012

Table 3. Model versus MOPITT CO annual mean bias for the Northern Hemisphere (NH), Southern Hemisphere (SH), and Global at 500 hPa. Annual mean spatial pattern correlation coefficients (r) between model and MOPITT CO global retrievals are in the right-most column.

	Bias (ppbv)			
Models	NH	SH	Global	r
CESM-CAM-superfast	−31.92	−17.65	−24.79	0.83
CICERO-OsloCTM2	1.56	6.99	4.28	0.86
CMAM	−13.68	−4.54	−9.10	0.93
EMAC	−1.79	2.24	0.23	0.93
GEOSCCM	−5.73	0.00	−2.86	0.87
GFDL-AM3	−9.01	0.58	−4.22	0.89
GISS-E2-R	19.23	25.64	22.43	0.91
GISS-E2-R-TOMAS	7.54	11.88	9.71	0.89
HadGEM2	3.05	6.40	4.73	0.76
LMDzORINCA	3.14	4.36	3.75	0.93
MIROC-CHEM	−12.57	−0.76	−6.65	0.92
MOCAGE	0.67	−2.46	−0.89	0.76
NCAR-CAM3.5	−12.59	−0.05	−6.32	0.87
STOC-HadAM3	7.37	11.22	9.31	0.85
TM5	−10.27	−1.33	−5.80	0.86
UM-CAM	13.24	21.27	17.26	0.89
MMM ± STD	−2.6 ± 12.4	4.0 ± 10.3	0.7 ± 11.2	0.87 ± 0.05

ACPD
12, 30755–30804, 2012

Table 4. Preindustrial (1850) to present-day (2000) changes in global mean tropospheric OH, tropospheric methane lifetime (τ_{CH_4}), CO and NO_x burdens, stratospheric ozone column (Strat O_3), humidity (Q), and temperature (T). Absolute changes in airmass-weighted temperature are given, while the rest of the quantities are expressed as percentage changes relative to 1850. Models that simulate reductions in present day OH relative to preindustrial are shown in bold. A cell with *** means that the model did not report that quantity.

Models	ΔOH (%)	$\Delta\tau_{CH_4}$ (%)	ΔCO (%)	ΔNO_x (%)	ΔStrat O_3 (%)	ΔQ (%)	ΔT (K)
CESM-CAM-superfast	6.1	−9.8	100.3	243.8	−7.6	8.1	1.4
CICERO-OsloCTM2	**−11.1**	**9.2**	**114.3**	**89.8**	**0.5**	**0.0**	**0.0**
CMAM	**−9.6**	**8.1**	**110.9**	**56.3**	**−3.2**	**8.3**	**1.2**
EMAC	**−7.6**	**2.1**	**102.1**	**63.4**	**−1.2**	**5.4**	**0.9**
GEOSCCM	**−12.7**	**12.0**	**120.3**	**62.5**	**−4.0**	**5.7**	**1.0**
GFDL-AM3	**−8.1**	**5.1**	**86.1**	**41.8**	**−2.4**	**3.4**	**0.6**
GISS-E2-R	7.0	−10.6	68.9	39.5	−6.1	5.8	0.9
GISS-E2-R-TOMAS	9.1	−11.7	71.1	33.6	−6.6	7.6	1.1
HadGEM2	**−0.7**	**−0.1**	**84.3**	**192.5**	**−6.0**	**3.3**	**0.5**
LMDzORINCA	**−5.9**	**4.1**	**94.8**	**87.0**	**0.3**	***	**0.8**
MIROC-CHEM	**−7.3**	***	**100.9**	**75.9**	**−3.1**	**4.7**	**0.8**
MOCAGE	14.6	−13.5	58.1	286.6	−19.7	5.2	0.9
NCAR-CAM3.5	11.7	−14.1	66.3	114.7	−3.3	6.9	1.1
STOC-HadAM3	3.2	−5.7	71.1	111.0	−4.0	3.5	0.6
TM5	**−4.3**	**1.2**	**94.1**	**67.7**	**0.6**	**0.0**	**0.0**
UM-CAM	6.0	−6.7	81.9	161.6	−6.1	3.5	0.6
MMM ± STD	−0.6 ± 8.8	−2.0 ± 8.8	89.1 ± 18.6	108.0 ± 75.4	−4.5 ± 4.8	4.7 ± 2.6	0.8 ± 0.4

ACPD
12, 30755–30804, 2012

Table 5. Same as in Table 4 but for changes in present day (2000) relative to 1980.

Models	ΔOH (%)	$\Delta\tau_{CH_4}$ (%)	ΔCO (%)	ΔNO_x (%)	ΔStrat O_3 (%)	ΔQ (%)	ΔT (K)
CESM-CAM-superfast	3.9	−5.0	5.3	-15.3	−3.7	3.7	0.6
CICERO-OsloCTM2	0.9	−1.3	6.2	3.5	0.1	0.0	0.0
CMAM	1.7	−2.8	7.9	0.4	−1.5	4.2	0.6
EMAC	3.8	−4.6	5.2	2.9	−1.4	3.9	0.6
GEOSCCM	0.6	−1.5	8.4	1.7	−2.7	2.8	0.5
GFDL-AM3	2.5	−3.6	5.5	3.6	−4.7	3.2	0.5
GISS-E2-R	6.9	−6.7	3.6	41.4	−6.4	2.7	0.4
GISS-E2-R-TOMAS	5.9	−6.7	3.5	14.3	−3.5	3.6	0.6
HadGEM2	3.8	−4.1	5.8	−1.2	−2.3	3.1	0.5
LMDzORINCA	1.4	−1.8	7.1	8.3	0.1	***	0.4
MIROC-CHEM	0.1	***	7.3	5.2	−2.4	0.1	0.0
MOCAGE	6.3	−5.9	1.3	−7.6	−8.7	2.0	0.3
NCAR-CAM3.5	5.9	−6.7	3.2	4.8	−2.0	4.1	0.7
STOC-HadAM3	4.4	−4.6	4.1	−2.2	−3.4	2.7	0.4
TM5	***	***	***	***	***	***	***
UM-CAM	4.8	−5.2	4.0	4.1	−3.6	2.7	0.5
MMM ± STD	3.5 ± 2.2	−4.3 ± 1.9	5.2 ± 2.0	4.3 ± 12.3	−3.1 ± 2.3	2.8 ± 1.3	0.4 ± 0.2

ACPD
12, 30755–30804, 2012

Table 6. Change in tropospheric methane lifetime due to climate change: difference between base 2000 time-slice and a simulation with 1850 climate (Em2000Cl1850). Change in tropospheric temperature and lifetime change per unit change in temperature are also shown for 10 models.

Models	$\Delta\tau_{CH_4}$ (yr)	ΔT (K)	$\Delta\tau_{CH_4}/\Delta T$ (yr K^{-1})
CESM-CAM-superfast	−0.27	1.4	−0.20
GFDL-AM3	0.12	0.6	0.21
GISS-E2-R	−0.76	1.1*	−0.69
GISS-E2-R-TOMAS	−0.70	1.1	−0.64
HadGEM2	−0.20	0.5	−0.40
MIROC-CHEM	−0.25	0.8	−0.30
MOCAGE	−0.20	0.9	−0.23
NCAR-CAM3.5	−0.37	1.1	−0.34
STOC-HadAM3	−0.46	0.6	−0.71
UM-CAM	−0.34	0.6	−0.55
MMM± STD	−0.30 ± 0.24	0.9 ± 0.3	−0.39 ± 0.28

* Temperature change is slightly different from that reported in Table 4 as a different control simulation was used to compare the Em2000Cl1850 simulation.

ACPD
12, 30755–30804, 2012

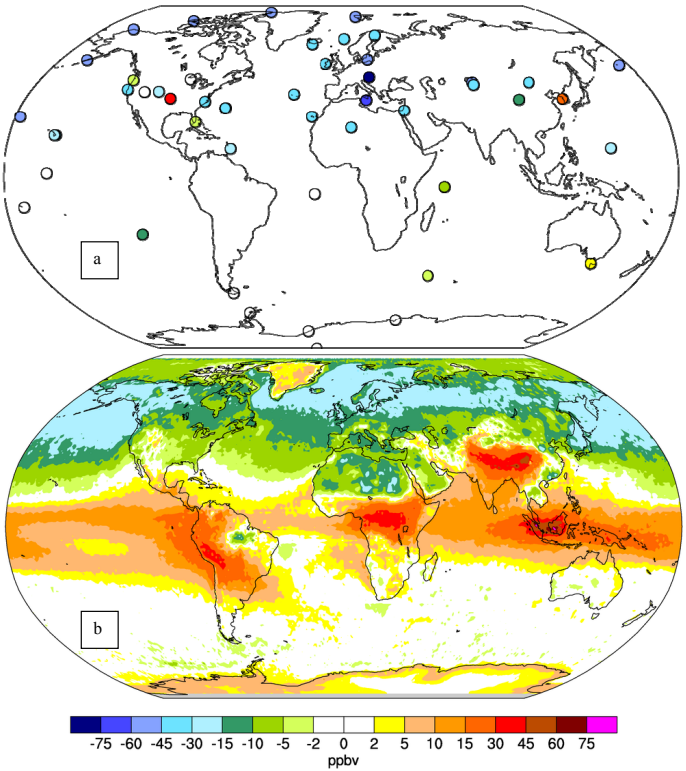

Fig. 1. Annual average bias of multi-model mean CO for 2000 against **(a)** surface CO observations averaged over the 1996 to 2005 period from the NOAA Global Monitoring Division (GMD) network (Novelli and Masarie, 2010; downloaded on 11 April 2012) and **(b)** average 2000–2006 MOPITT CO at 500 hPa. Each circle in **(a)** indicates the mean bias at the CO measurement site. For comparison with satellite observations in **(b)**, each model was convolved with the MOPITT operator (a priori and averaging kernels) before taking the difference.

ACPD
12, 30755–30804, 2012

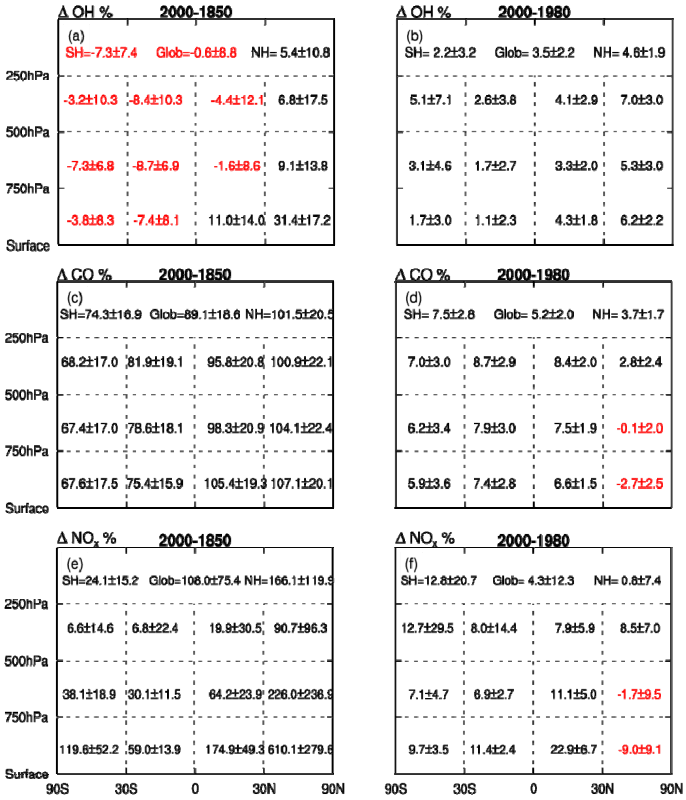

Fig. 2. Multi-model mean percentage change in tropospheric OH, CO and NO_x burdens, humidity (Q), and absolute change in temperature for 12 subdomains of the atmosphere as defined by Lawrence et al. (2001) for 2000–1850 (left) and 2000–1980 (right). Negative values are highlighted in red. Changes in the mean global, Southern Hemisphere (SH), and Northern Hemisphere (NH) troposphere (surface to 200 hPa) are shown in the topmost row of each plot.

ACPD
12, 30755–30804, 2012

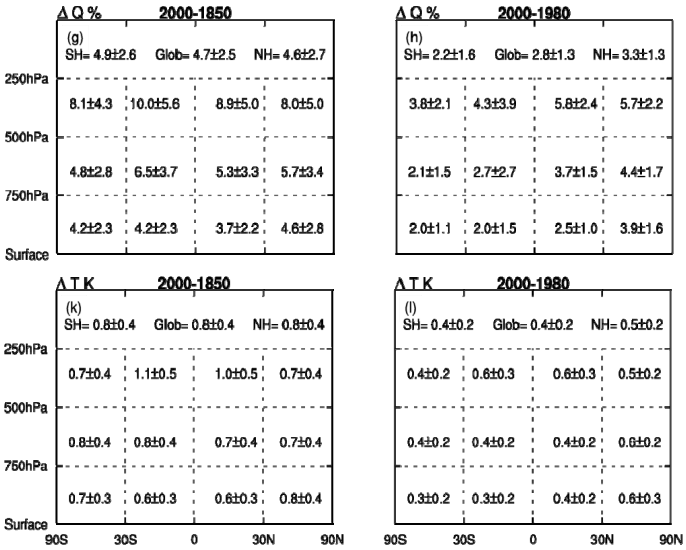

Fig. 2. Continued.

ACPD
12, 30755–30804, 2012

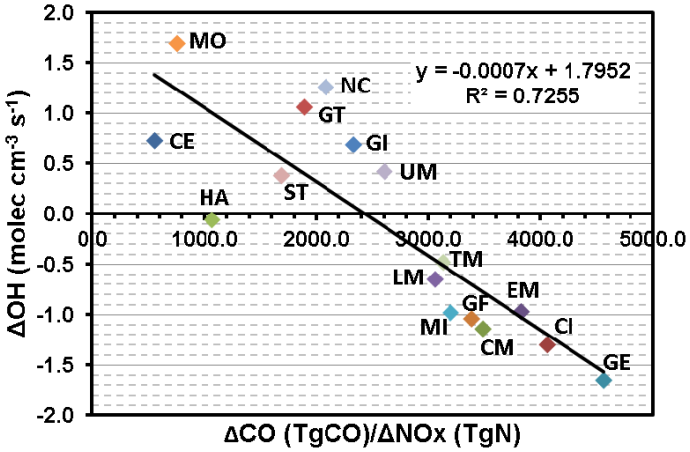

Fig. 3. Scatterplot of absolute change in annual average tropospheric mean OH concentration from preindustrial (1850) to present-day (2000) versus the ratio of absolute changes in annual average total tropospheric CO and NO_x burdens for each of the 16 models. Each model data point is denoted by the first two letters of the model name shown in Table 1. Solid line corresponds to a linear regression of changes in OH with the ratio of changes in CO and NO_x burdens. The regression equation is shown on the upper right corner of the plot.

ACPD
12, 30755–30804, 2012

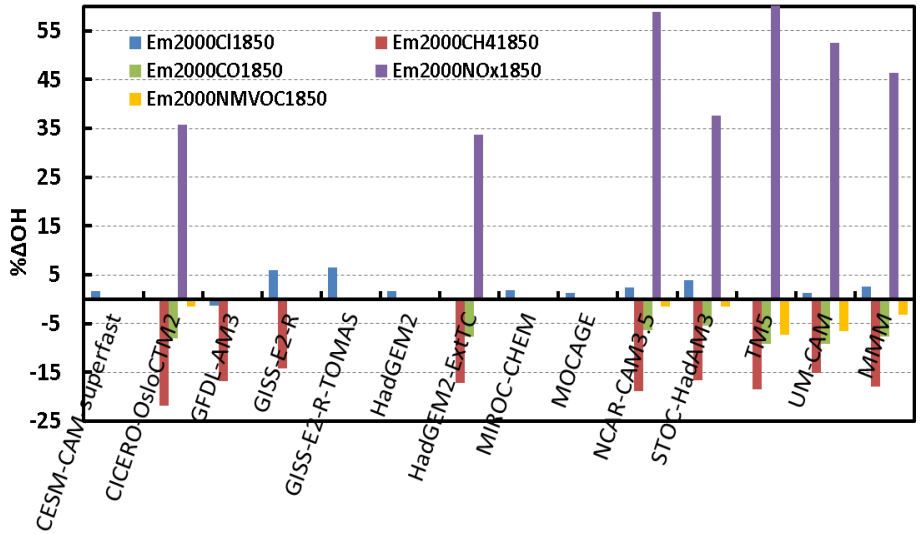

Fig. 4. Percent tropospheric mean OH concentration change due to preindustrial to present-day changes in climate (Em2000Cl1850), methane burden (Em2000CH41850), and anthropogenic emissions of CO (Em2000CO1850), NO_x, (Em2000NOx1850), and NMVOCs (Em2000NMVOC1850). The multimodel mean OH changes for each experiment are also shown (MMM).

ACPD
12, 30755–30804, 2012

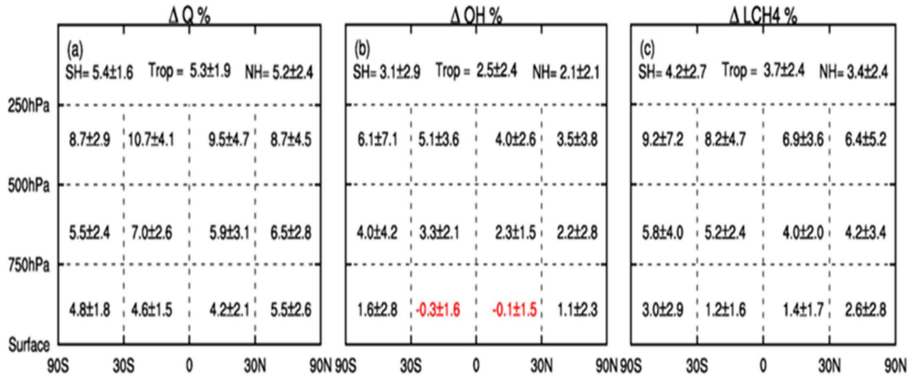

Fig. 5. Percent change in multi-model mean (10 models) regional **(a)** specific humidity, **(b)** tropospheric OH and **(c)** methane loss flux due to climate change only (2000-Em2000Cl1850).

ACPD
12, 30755–30804, 2012

Fig. 6. Percent change in multi-model mean OH in 12 subdomains of the atmosphere for 2000 relative to attribution experiments: **(a)** Em2000CH41850 (8 models), **(b)** Em2000CO1850 (6 models), **(c)** Em2000NOx1850 (6 models), **(d)** Em2000NMVOC1850 (6 models).

ACPD
12, 30755–30804, 2012